University of Glasgow

DEPARTMENT OF

AEROSPACE ENGINEERING

A Preliminary Study Of The Flow Around A Delta Wing Using High Resolution Pressure Measurements.

M. Jupp[1], F. Coton[2] and R. Green[3]

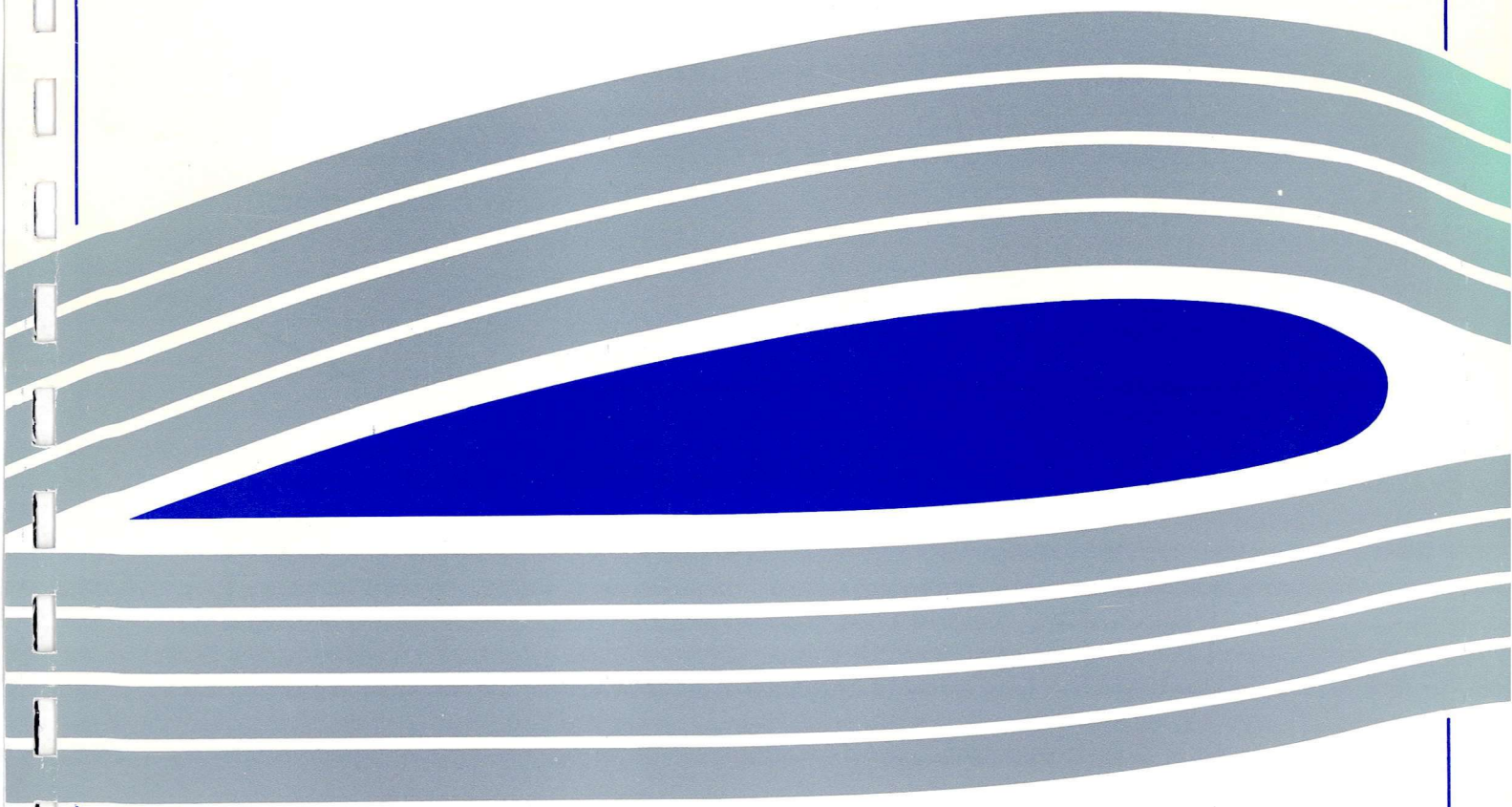

G.U. Aero Report No. 9720

A Preliminary Study Of The Flow Around A Delta Wing Using High Resolution Pressure Measurements.

M. Jupp[1], F. Coton[2] and R. Green[3]

Department of Aerospace Engineering

James Watt Building South

University of Glasgow

Glasgow G12 8QQ

October 1997

---

[1] Research Student
[2] Senior Lecturer
[3] Lecturer

SUMMARY

A study of the flow around delta wings has been carried out in a series of experiments in the University's Handley-Page Wind-Tunnel facility. The objective of the experiments was to capture high spatial and temporal resolution pressure measurements on a specially designed 60° delta wing model. This project has been devised to analyse the results of the study with a view to determining a reliable method of vortex breakdown detection on delta wings using data obtained from pressure measurements alone. A fundamental requirement of the proposed method is that it should apply equally under static and dynamic conditions.

In order to achieve the aim of the project, a broad understanding of the physics of vortical flows is required. This is to be achieved in two ways; firstly, by carrying out a literature research exercise on the nature, causes and effects of vortex breakdown, secondly, to validate the findings of the pressure data analysis by carrying out further experiments using smoke visualisation techniques.

The findings of the literature research exercise are presented, together with a description of the wind-tunnel experiments and the preliminary results from the analysis of the pressure data. The models to be used in the forthcoming smoke-visualisation experiments have been built and a series of tests have been carried out to evaluate their design. A description of the smoke tunnel models and the results of these tests are also presented.

The work of this project has so far highlighted a number of issues to be dealt with in future research as part of this project. To conclude this report, a series of proposals are presented detailing the work required to resolve these issues.

List Of Contents **Page**

continued...

List Of Contents (Cont.) **Page**

List Of Figures

continued...

List Of Figures (Cont.) **Page**

continued...

List Of Figures (Cont.) **Page**

1. INTRODUCTION

The aim of the following chapter is to provide an introduction to a current research project aimed at investigating the low-speed aerodynamic characteristics of delta wings with particular reference to vortex breakdown. The chapter is divided into two sections; the first sets out the aims and objectives of this report and the project as a whole, the second introduces vortical flows on delta wings and their relationship to vortex breakdown.

1.1 Aims & Objectives

The principle aim of the work is to determine a reliable method of vortex breakdown detection using pressure measurements. A requirement of the method is that it should be applicable to both static and dynamic flows. To achieve this, the objectives of the project are firstly, to gain an understanding of vortical flows and the nature, cause and effects of vortex breakdown as applied to delta wings by carrying out a literature research exercise. Secondly, to analyse pressure data, obtained at high spatial and temporal resolution on a specially designed 60° delta wing model, from experiments carried out in the University of Glasgow's Handley-Page Wind-Tunnel facility. The results from this analysis will subsequently be validated by carrying out further experiments using smoke visualisation techniques.

The aim of this report is to detail the work carried out over the previous eleven months as part of an ongoing research project investigating vortex breakdown on delta wings. The report is presented as a series of distinct sections. Chapter Two presents the findings of the literature research exercise and Chapter Three describes the Handley-Page Wind-Tunnel experiments. A report on the progress of the data analysis is provided in Chapter Four and the smoke flow visualisation experiments are described in Chapter Five. Finally, the objectives of the project for the next twelve months are outlined in Chapter Six.

1.2 Delta Wings

The flow structure on a delta wing at moderate to high angles of attack is extremely complex. The flow is dominated by a pair of vortical structures, known as the primary vortices, the centrelines of which extend from the wing apex into the wake beyond the trailing-edge of the wing, along a ray located somewhere inboard of each leading-edge. The location and height above the wing of each centreline is chiefly dependent on angle of attack (α), the sweep angle (Λ) and the shape of the leading-edge[1].

These primary vortices are formed when the attached approach flow on the lower surface of the wing turns outboard and heads towards the leading-edge. Unable to negotiate this sharp turn, the flow separates from the lower surface and forms a free shear layer or vortex sheet. The combined influence of the bound vorticity in the shear layer and a spanwise pressure gradient, (which, on the leeward surface is positive towards the wing centreline), results in the shear layer moving around the leading edge and inboard over the top surface of the wing, rolling up in a spiral fashion to form concentrated vortex cores with distributed vorticity (Figure 1.1). Although this vorticity is fed into the vortex continuously along the length of the leading-edge, it is also continuously transported downstream along the vortex core and shed from the trailing-edge, thus enabling the vortex to remain stationary above the wing surface providing a useful and stable device for generating lift.

The creation of primary vortices causes the attached boundary layer underneath each structure to turn outboard towards the leading-edge. This outflow meets the same spanwise pressure gradient, which of course, is adverse in the direction of the leading-edge, causing the flow to separate into a secondary shear layer. This, in turn, rolls up into a secondary vortex structure rotating in opposition to it's primary parent (Figure 1.2). The main effect of the secondary vortex is to displace the primary vortex upwards and inwards, the effect being greater if the boundary layer is laminar, where separation occurs earlier, increasing the size of the secondary vortex structure.

[1] Lowson (1963), (1991)

Aircraft utilising delta wings can be designed such that they are able to generate lift in the conventional sense using camber, twist, small angles of incidence etc. However, at higher angles of incidence where vortices form, additional lift and it's corresponding drag penalty are generated because the highest velocities of the flow, at the periphery of the vortex core, can be as much as three times that of the freestream[1]. The associated low pressures generated by this increased flow velocity increasingly dominate the total lift curve of the wing as the angle of attack is increased to high values (Figure 1.3).

However, at some value of alpha and at some point along the vortex core, a sudden transformation takes place causing the axial velocity of the flow to stagnate and the vortex to breakdown into large scale turbulence. It is the study of this vortex breakdown phenomenon that is central to the theme of this research.

[1] Lambourne & Bryer (1961)

2. VORTEX BREAKDOWN - PREVIOUS WORK

The aim of the following chapter is to highlight the most significant observations made during some forty years of research into the nature, cause and effects of vortex breakdown. The chapter is divided into two sections; the first dealing with the results and conclusions drawn from experimental investigations and the second covering the most significant theories that have attempted to explain and predict vortex behaviour.

2.1 Experimental History

The first observation of vortex breakdown on a delta wing was reported by Peckham & Atkinson in 1957[1]. Subsequent articles[2] independently showed that the position along the vortex at which breakdown occurs depends primarily on a combination of leading-edge sweep and angle of incidence. For a given delta wing at low angles of incidence, the breakdown occurs in the vortex some way downstream of the trailing-edge. With an increase in angle of incidence or a decrease in sweep, however, the breakdown moves upstream until it reaches the trailing-edge of the wing. With a further increase in alpha, the breakdown point moves upstream towards the wing apex resulting in a loss of lift. Since the first discovery of the vortex breakdown phenomenon, a vast number of articles and papers have been presented detailing experiments which have been carried out to determine it's nature, causes and effects. The following is a summary of the work directly relevant to the current research.

In 1961, Lambourne & Bryer[3] described experiments on a delta wing using both surface-oil and dye-injection visualisation together with relatively crude pressure measurements. As a result of these experiments, vortex breakdown was described as:

> "a structural change at some position along a vortex from a strong regular spiral motion to a weaker turbulent motion".

[1] Peckham & Atkinson (1957)
[2] Peckham (1958), Elle (1958)
[3] Lambourne & Bryer (1961)

This change was characterised by:

1. A sudden deceleration of the flow along the vortex axis.

2. The expansion of the vortex core

3. Breakdown to large scale turbulence which resembles the wake behind a bluff body.

[Note - The deceleration and expansion of the vortex core takes place over a finite length of the vortex axis and this has led to problems in defining the vortex breakdown position. More recent work assumes a breakdown region which extends to five or six times the vortex core diameter.]

Lambourne & Bryer observed two distinct types of breakdown, first reported by Harvey[1] a year earlier. Both share the characteristics of sudden deceleration and breakdown to turbulence, however it is the expansion of the vortex core that defines each type. Spiral, or S-type breakdown (Figure 2.1), is an asymmetric spiralling of the vortex core which remains intact for a few turns of the spiral before breaking down into turbulence. Bubble, or B-type breakdown (Figure 2.2), is an axisymmetric diffusion of the vortex core over an bubble-shaped region with an open downstream end into which the flow recirculates before either; immediately breaking down into turbulence, or reforming into a vortex core briefly before breaking down again in a Spiral fashion.

Lambourne & Bryer stated that the S-type breakdown was more commonly observed on delta wings with the B-type appearing occasionally and then only briefly before taking up the spiral form. However, other observers notably Parker[2], have since only observed B-type breakdown on delta wings, this observation will be discussed in Chapter 6.

---

[1] Harvey (1960)
[2] Parker (1976),

[Note - The majority of research into the nature of vortex breakdown has been carried out in diverging-tube experiments using water and dye visualisations. This is because it is considered that the essential parameters such as Reynolds number, swirl magnitude and downstream pressure gradients are more easily controlled in a confined environment. A series of experiments were reported by Faler & Leibovich[1], who, by varying the inlet swirl angle and/or Reynolds number, were able to identify a total of six different classes of breakdown, the S-type and B-type being the most common with the other four types sharing the characteristics of these two.]

From their experiments, Lambourne & Bryer were able to draw a number of conclusions:

1. An essential feature in the presence of vortex breakdown is a very low total pressure of the flow close to the vortex axis which means that the axial flow is easily brought to rest by any adverse downstream pressure gradient.

2. The vortex breakdown position is sensitive to the pressure gradient along the core of the vortex, i.e. an increasing pressure gradient tends to precipitate breakdown.

3. For delta wings with sharp leading edges, the position of vortex breakdown for a given sweep angle and angle of incidence is largely independent of Reynolds number in the range $0.01 \times 10^6 \leq Re \leq 4.6 \times 10^6$.

4. The presence of burst above the wing causes a loss of suction locally at the surface and a modification to the position of separation of the surface flow beneath the vortex.

Payne et al[2] observed that for a delta wing, the lift, drag and pitching moment all undergo an abrupt deterioration as the location of vortex breakdown moves upstream over the trailing edge of the wing (Figure 2.3), as well as a sudden change in the

[1] Faler & Leibovich (1977)
[2] Payne, Ng & Nelson (1986)

mean axial velocity profile from a jet-like profile upstream of breakdown, to a wake-like profile downstream (Figure 2.4). These effects having first been identified separately by Hummel and Srinivasan[1] and Faler and Leibovich[2] respectively. The latter being observed in confined diverging-tube experiments.

Gad-El-Hak & Ho[3] used smoke visualisation to identify a hysteretic phase lag in the formation of the primary vortex and it's eventual breakdown when compared to the static case at a given incidence, as a delta wing is oscillated in pitch. Later, Atta & Rockwell[4] focused their attention on the secondary vortex, where a similar hysteretic lag was observed and it was shown that the secondary vortex system breakdown always precedes that of the primary. It was shown by Jarrah[5], using six-component airload measurements, that the hysteretic lag, first observed by Gad-El-Hak & Ho, also occurred in the corresponding values of lift, drag and pitching moment. Perhaps most importantly for this research, this effect was also identified in pressure measurements reported by Thompson et al[6]. The degree of lag in each of these cases being chiefly dependent on the frequency of oscillation, even to the extent that the lag can be as much as 180°, (i.e. the lift generated by the wing can be at a maximum at the incidence corresponding to minimum lift in the static case and visa versa). Coming full circle in this particular area of research, Gursul & Yang[7] have suggested that this phase lag is very closely associated to the external pressure gradient generated by the wing. This is consistent with the conclusions drawn by Lambourne & Bryer[8].

The previous work described here is merely a representative sample of the experimental research into the causes and effects of vortex breakdown. Many other papers[9] have highlighted the effects of a range of parameters that are known to affect the phenomenon. It is not proposed to go into any further detail in this report, as a

[1] Hummel & Srinivasan (1966)
[2] ibid.
[3] Gad-El-Hak & Ho (1985)
[4] Atta & Rockwell (1990)
[5] Jarrah (1989)
[6] Thompson, Batill & Nelson (1990)
[7] Gursul & Yang (1995)
[8] ibid.
[9] See Appendix A

number of excellent revue papers[1] have already completed this task. However, a listed summary of the most significant previous experimental work is given in Appendix A.

2.2 Theories of Vortex Breakdown

Alongside the experimental observations made since the late fifties, a number of papers have been published[2] putting forward a series of theoretical explanations for the nature and causes of vortex breakdown. Theoretical studies can be categorised roughly according to whether breakdown is considered to be associated with:

1. Instability	a. axisymmetric disturbances
	b. spiral disturbances
	c. non-linear interactions
2. Stagnation	a. separation analogy
	b. failure of slender core/quasi-cylindrical approximation
	c. numerical failure
3. Wave phenomena	a. solitary/inertia waves
	b. transition between conjugate-flow states
	c. shock/hydraulic jump analogy
4. Vorticity	a. negative azimuthal vorticity

The following section is divided into four sub-sections, each describing a category of theory as described above. It is proposed in this report to explain only the main points of these theories as the detail has already been described in a series of revue articles[3]. Before discussing any of them at all, it should be noted that the following assumptions are common to practically all theoretical analyses, although the first two are

[1] Escudier (1988), Magness (1991), Mabey (1991), Ashley et al (1991), Nelson (1991), Delery (1994), Yegna Narayan & Seshadri (1996),
[2] See Appendix B
[3] Hall (1972), Parker (1976), Faler & Leibovich (1977), Leibovich (1978), (1984), Escudier (1988), Spall et al (1987), Brown & Lopez (1990), Mabey (1991), Hemsch & Luckring (1990), Nelson (1991)

sometimes relaxed in direct numerical computations:

1. Cylindrical mean flow, i.e. slow variations in core diameter are neglected.

2. Inviscid flow

3. Incompressible flow

4. Laminar flow

5. Steady flow

2.2.1 Instability

Jones[1] was the first to suggest that hydrodynamic instability might be responsible for vortex breakdown. The theory is based on a linear stability analysis applied to the axisymmetric laminar Navier-Stokes equations. However, Jones was unable to define a criterion that could be applied generally. The idea was later pursued by Ludwieg[2] who suggested that after the onset of instability, spiral disturbances could amplify, induce an asymmetry in the vortex core and subsequently lead to stagnation.

Lessen et al[3] studied the inviscid stability of the Q-vortex to infinitesimal non-axisymmetric disturbances with normal modes of the following form:

$$(\exp[i(\kappa\chi - n\theta - \kappa\gamma t)]$$

where: κ = axial wave number, χ = axial co-ordinate,
θ = azimuthal co-ordinate, γ = complex phase velocity

For negative wave-numbers (i.e. helical wave paths opposite in sense to the vortex rotation) the amplification rate increases with respect to swirl parameter (q) to a maximum at $q = 0.85$ and decreases again becoming negative at $q > 1.58$ whereafter the flow is stable to all disturbances.

---

[1] Jones (1960)
[2] Ludwieg (1965)
[3] Lessen et al (1974)

Garg & Leibovich[1] and Escudier et al[2] have both reported values of q which result from fitting Q-vortex velocity profiles to their experimental data for flows exhibiting breakdown. Garg & Leibovich found that q = 0.8 was the smallest value at any location, whereas upstream of breakdown it was always significantly greater than 1.5 and downstream it was less than 1.5. It was claimed that this suggests stability to axisymmetric disturbances everywhere, and an instability to helical disturbances downstream of the breakdown region. In all theories of hydrodynamic instability, breakdown is analogous to laminar-turbulent transition.

2.2.2 Stagnation

One feature of the flow that has already been described as an essential aspect of vortex breakdown is the deceleration and eventual stagnation of the flow at the vortex axis. Polhamus[3] was the first to develop a theory using the analogy of a two-dimensional laminar separation and reattachment bubble when regarding the separation and subsequent reattachment of the flow over delta wings. This theory can be used to predict the low-speed lift and drag-due-to-lift characteristics of sharp-edged delta planforms. A significant deviation of experimental results from theoretical results being indicative of vortex breakdown.

A number of investigators have carried out numerical calculations of the axial development of the vortex flow and have identified vortex breakdown as occurring at the location where a rapid divergence of the numerical calculation takes place. The majority of investigators[4], in adopting this technique, use the quasi-cylindrical form of the equations of motion, the investigations of Gartshore and Mager being of the momentum-integral type, whereas Bossel uniquely divided the flow in the vicinity of breakdown into four regions which he then matched together. Hall on the other hand, using this technique was first to demonstrate that the axial pressure gradient is composed of two components: the imposed external pressure gradient plus the swirl contribution. On the other hand, those investigators[5], who have not used the quasi-cylindrical approximation, have tended to confine themselves to calculations

[1] Garg & Leibovich (1979)
[2] Escudier et al (1982)
[3] Polhamus (1971)
[4] Gartshore (1962), Hall (1964), Bossel (1969), Mager (1972),
[5] Kopecky & Torrance (1973), Grabowski & Berger (1976).

involving laminar flow using the full Navier-Stokes equations, subject only to restrictions of axial symmetry, steadiness and incompressibility.

2.2.3 Wave Phenomena

Squire[1] was the first to attempt to connect vortex breakdown with wave-motion. He considered the possibility of the existence of standing waves on a cylindrical vortex motion for which the stream function satisfies the following equation for inviscid flow:

$$\frac{\partial^2\psi}{\partial x^2} + \frac{\partial^2\psi}{\partial r^2} - \frac{1}{r}\cdot\frac{\partial\psi}{\partial r} = \frac{r^2}{\rho}\cdot\frac{dH}{d\psi} - \frac{1}{2}\cdot\frac{dK^2}{d\psi}$$

where: (for inviscid flow) the total head H and circulation $2\pi K$ are functions of ψ alone.

Squire assumed that if standing waves could exist, then small disturbances coming from downstream will propagate in the upstream direction and ultimately provoke breakdown. He proposed that for a 'supercritical' flow, long waves propagating against the flow are carried downstream and do not affect events in the upstream direction, whereas for a 'subcritical' flow, long waves may propagate upstream, and hence for some limit situation, standing waves can exist on the flow.

Benjamin[2] on the other hand proposed that vortex breakdown is a transition between two conjugate swirling flow states A and B, each of which is a solution of the equation for inviscid cylindrical flow:

$$\frac{\partial^2\psi}{\partial r^2} - \frac{1}{r}\cdot\frac{\partial\psi}{\partial r} = \frac{r^2}{\rho}\cdot\frac{dH}{d\psi} - K\cdot\frac{dK^2}{d\psi}$$

Benjamin showed that if flow A is supercritical then flow B is sub-critical in direct analogy with the shock/hydraulic jump in open channel flow. The critical state theory is based on the assumption that a columnar vortex can support axisymmetric standing waves. Benjamin, like Squire before him, found that the critical condition for the

[1] Squire (1960)
[2] Benjamin (1962)

existence of standing waves is :

$$\text{Swirl Ratio } (\alpha_0) = \frac{V_\theta}{V_x} \geq 1.2$$

By decreasing the axial velocity component, or by increasing the swirl velocity component, (i.e. by increasing α and/or decreasing Λ), a supercritical flow is driven towards subcritical. Thus, if this assumption is correct, vortex breakdown can be thought of as the ability or not of the flow to sustain standing waves.

2.2.4 Azimuthal Vorticity

A number of investigators[1] have highlighted the importance of vorticity in determining vortex breakdown. Their observations have shown that the onset of negative azimuthal vorticity, (i.e. the swirl ratio of velocity (α_0) exceeds the swirl ratio of vorticity (β_0)), is a necessary condition for the onset of breakdown. In fact, the attainment of zero or negative axial velocity is only possible if azimuthal vorticity becomes negative. Nelson & Visser have examined this theory experimentally, whilst Brown & Lopez have tested this condition against numerical Navier-Stokes equations of swirling pipe flow and found the numerical solution would diverge rapidly only if :

$$\tau_0 = \frac{\alpha_0}{\beta_0} > 1$$

Boffadossi used the theory originated by Brown & Lopez to develop a criterion for vortex breakdown using a computational method based on the unsteady formulation of a non-linear vortex-lattice scheme. This scheme used Rankine vortices with a viscous core diffusion model physically consistent with the turbulent diffusion mechanism of continuous shear layers. In his paper, Boffadossi predicts vortex breakdown for a series of thin delta wings and plots his results against a series of experimental data to very good effect.

This concludes the treatment of theoretical investigations into vortex breakdown as part of the literature research exercise, a listed summary of previous theoretical work is given in Appendix B.

[1] Brown & Lopez (1990), Nelson & Visser (1991), Boffadossi (1996)

3. WIND-TUNNEL EXPERIMENTS

The following chapter describes the experiments carried out at Glasgow University's Handley-Page wind-tunnel facility using delta wing models. The chapter is divided into four sections describing; the models used, the wind-tunnel, the data acquisition system and the experimental procedure.

3.1 The Model

A model was specially designed and built at Glasgow University. The plain delta wing was machined from a solid block of aluminium with a root-chord, (c) of 800mm, and a sweep angle, (Λ) of 60°. This gave an aspect ratio, (AR) of 2.31 and a span-width (2s) of 923.8mm. The model had a flat leeward surface, a highly contoured windward surface and a bevelled edge on the windward side to produce sharp leading and trailing edges (Figure 3.1). The model was able to accommodate 192 Kulite Type CJQH-187 differential transducers located primarily on the starboard side of each surface, (Figure 3.2). The wing had a thickness ratio of 9.0%, which is high compared with the previous work studied (range - 0.1% to 5.9%).

The model was designed such that the standard nose-section could be removed and replaced with a rounded nose-section, (Figure 3.3). The rounded nose had a radius of 50mm and had the effect of reducing the root chord by 6.25%. It had a bevelled leading-edge similar to it's standard counterpart and provided, along with the unusual shape of the windward surface, a unique opportunity to investigate the effect on vortex formation and breakdown.

3.2 The Wind-Tunnel Facility

The Handley-Page wind-tunnel facility, located at the University's Spencer St. Annex, is a closed return type with an octagonal test section measuring 2.13m by 1.61m (working area = 2.667m^2) giving a span to tunnel width ratio[1] of 0.434 and a model blockage of 2.5% to 8.9% over the alpha range $0° \leq \alpha \geq 42°$ (not including strut fairings). The model was mounted leeward side up, supported on three struts and pivoted about the forward strut at a chord position of 0.25c. The forward strut was

[1] As per Weinberg (1992)

connected to the main support structure whilst the two rear struts were connected to the actuation mechanism situated below the tunnel floor.

Movement of the model was achieved by displacement of the two rear struts using a Parker 2H Series linear hydraulic actuator and crank mechanism. The system used a high response proportional directional control valve with a E200-595 PID analogue closed loop controller and could deliver a maximum thrust of 17.0KN during extension and 6.53KN during retraction at a piston speed of 1.1m/s. An angular displacement transducer mounted on the crank was used to provide a feedback signal and for recording the instantaneous angle of attack.

The required motion profile was provided by an AMSTRAD 1512 microcomputer equipped with an ANALOG DEVICES RT1815 multi-function input/output board. The required output function was digitised into equal time steps and the frequency was controlled using interrupts on the AMSTRAD microcomputer. The computer programme was written in TURBO PASCAL.

3.3 The Data Acquisition System

Data acquisition was carried out by a PC equipped with a 486 processor, using TEAM 256 software. The PC was configured and interfaced with propriety Bakker Electronics BE256 modules which provided the necessary analogue to digital conversion. The system had 200 channels, each capable of sampling at 50kHz, giving an overall sampling rate of 10MHz. The channels not taken up by transducers were used to sample temperature, barometric pressure, working section static pressure, reference dynamic pressure and incoming velocity.

The pressure transducers fitted to the model had one side of the pressure diaphragm open to the ambient pressure outside the wind-tunnel, whereas the reference dynamic pressure in the wind-tunnel working section was determined by measuring the difference between working section static pressure upstream of the wing apex and settling chamber static pressure. The pressure tappings were connected to a FURNESS FC012 micromanometer, providing an analogue signal for the data acquisition unit.

The signals from each transducer were delivered to a specially designed signal conditioning unit of modular construction, each module containing it's own control board. On instruction from the computer, the control board automatically moved all offsets to below the A to D converter resolution and adjusted all gains as necessary. During each test run the computer sampled the minimum and maximum output of each transducer and adjusted the gains automatically as required.

3.4 Experimental Procedure

Four types of motion were tested out in this study. These were; 'static', 'ramp up', 'ramp down' and 'oscillatory'. Similar series of tests were carried out using the delta wing in each nose-section configuration. Each test was given a unique identification number denoting the model number, (i.e. sharp or round nose configuration), the motion type and the version number, (i.e. an unsatisfactory run may have to be repeated - this avoids having to renumber a run which uses the same parameters).

For the static tests (motion type = 0), the wing was set at a starting incidence of -5° (Table D.1)[1]. The wing was then pitched-up in 1° increments to + 42°. A suitable period was allowed prior to data collection at each incidence and then pressure data were sampled at a frequency of 2.0 kHz for a period of 1s. The total data set was divided into three 'runs' each covering an arc of 16°, giving a data set of 32000 samples per run.

A ramp test programme (motion type = 2 / 3) was conducted to examine the effect of pitch rate on wing performance (Tables D.3 and D.4)[1]. In these tests, the wing was set at a starting incidence of -5° / 40° and pitched-up or down at a constant pitch rate over an arc of 45°. Some 8000 samples of pressure data were collected during each cycle and the ramp motion was repeated over several cycles. Data from four cycles of motion were recorded at each pitch rate to give a total of 32000 samples over the range of alpha under consideration.

[1] See Appendix D

For the oscillatory test programme, the wing was pitched over a range of mean incidences and reduced frequencies (Table D2)[1] at a peak amplitude of 10° or 20° to determine the effect of each on wing performance. Some 4000 samples of pressure data were collected during each cycle and the sinusoidal motion was repeated over several cycles. Data from eight cycles of motion were recorded at each level of reduced frequency, again to give a total of 32000 samples per data set.

[1] See Appendix D

4. DATA ANALYSIS

The following chapter details the data analysis work carried out so far. The chapter is divided into two sections; the first details the analysis methods, the second provides a summary of results so far.

4.1 Analysis Methods

All of the binary data collected by the data acquisition system were stored on the PC prior to being downloaded onto DAT tape through a HP35470A DAT drive. Raw data were then reduced using a dedicated code written in C. The reduced data were stored as ASCII files identified by a run number, each file being made up of a run information block (Table C.1), and 200 channels x 32000 records of reduced data.

As part of the current study, a series of dedicated programmes have been written in FORTRAN 77 to manipulate and prepare the data for presentation and analysis. The programmes have the capability to average the data and calculate pressure, force and moment coefficients or RMS pressure values. The facility to interpolate for values at the leading and trailing edges as well as areas on the wing with low transducer density is also included.

A PV-WAVE software suite. has also been written to allow the further manipulation and presentation of the data in a number of formats. These include: two-dimensional line plots, 2-D contour plots and 3-D 'carpet' plots. Details of specific routines and results are given in the following section.

4.2 Results Of The Preliminary Analysis

All plots made so far have used data obtained from the series of static tests, (run nos. 18000011, 18000021 and 18000031 - see Table D.1 for details), carried out on the delta wing in it's sharp-nosed configuration. The following section is divided into six sub-sections each detailing a sub-group of plots.

4.2.1 C_P v x/c, z/s

A series of plots have been made of mean C_P against non-dimensional chord length (x/c) for each span station. Figure 4.1 presents two plots showing four values of alpha overlaid upon one another to show the overall trend of the chordwise C_P distribution. Alternatively, Figure 4.2 shows a single plot of eight alpha values, offset one above the other to clearly show the effect on the chordwise C_P distribution of increasing the wing incidence. The trend apparent from the C_P v x/c plots was that, for a given span station at positive values of alpha, the measured value of negative C_P tended to be greatest at the apex of the wing decreasing towards the trailing-edge (Figure 4.1).

A second series of plots have been made of mean C_P against non-dimensional half-span (z/s). The format of the plots was similar to those described above, with each plot showing the spanwise distribution of mean C_P at each chord station. The C_P v z/s plots showed that, for a given chord station at positive values of alpha, the measured value of negative C_P was at it's lowest along the centreline of the wing. The C_P trace was seen to form a 'suction peak' at approximately $z/s = 0.7$ before falling off again at the leading-edge (Figures 4.3 & 4.4). It was apparent that the suction peak was more pronounced at the wing apex and reduced in effect towards the trailing edge. Meanwhile, an increase in alpha was seen to increase both the magnitude and width of the suction peak particularly at the lower chord stations.

A third series of plots used the same data as above, to create two-dimensional contour plots of the C_P distribution on the leeward surface of the wing. Figure 4.5 shows four plots of the C_P distribution covering a range of values of alpha. These plots were designed to show the entire C_P distribution with increasing wing incidence.

4.2.2 RMS v x/c, z/s

Two-dimensional line plots and contour plots were made of calculated RMS pressure against x/c and z/s using a similar technique to that employed in the previous sub-section.

The trend evident from the RMS v x/c plots (Figure 4.6) showed that, for a given span station at positive values of alpha, there was an increase in RMS activity along the length of the wing from the apex to the trailing-edge. The peak of this RMS activity occurred at approximately $x/c = 0.8$ before dropping off again towards the trailing edge. The RMS activity, as well as the rate of increase of RMS with chord station, was seen to increase with an increase in alpha.

The RMS v z/s plots showed that, for a given chord station, at positive values of alpha, the minimum RMS activity occurred at the wing centreline with a main peak occurring in the range $0.4 < z/s > 0.6$. This was followed by a local minimum value and a secondary peak occurring in the range $0.75 < z/s > 1.0$ (Figure 4.7). Towards the apex of the wing this secondary peak occurred at, or possibly outboard of, the leading-edge. However, with an increase in alpha and chord station, both peaks were seen to move inboard and were seen to increase in magnitude and width, an observation that was also evident in the corresponding contour plots (Figure 4.8).

4.2.3 Min, Max & Average C_P v Alpha, x/c

The information provided in Figures 4.3 and 4.4 represents the spanwise C_P distribution at a given chordal location. These data were interrogated further to provide the maximum, minimum and average C_P values at each chordal position. The variation of these parameters with incidence could then be plotted and compared. As an example, Figure 4.9 shows the variation of the maximum, minimum and average C_P values at chord stations 4 ($x/c = 0.2$) and 5 ($x/c = 0.275$) against incidence. These plots illustrate the general trend of these parameters at all chordwise stations. In particular the maximum C_P value tended to decrease with an increase in incidence as did the average C_P. The minimum C_P value followed the same trend until a peak suction was attained . After this, the suction decreased with increasing incidence as alpha was increased further (Figure 4.9). In contrast, towards the trailing edge, all

three values of C_P at a given angle of attack were seen to reduce in magnitude and the peak suction, when still apparent, was seen to occur at a lower incidence.

An alternative way of representing the above data is presented in Figure 4.10. Here, the variation of the parameters with chordwise position are plotted at two angles of attack. In each case, the suction is greatest at the apex of the wing and decreases steadily to a minimum at the trailing-edge. As alpha is increased, all three values of C_P at a given chord station tend to increase.

4.2.4 Min, Max & Average RMS v x/c

Using a similar technique to that detailed in the previous sub-section, the mean RMS pressure values were manipulated to obtain the minimum, maximum and non-dimensional average spanwise RMS values for each value of alpha. These were then plotted against x/c. The PV-WAVE routine used to plot these graphs was designed in such a way as to be able to select a specific span range of RMS values to be manipulated. This was done because the previous plots of RMS v x/c and z/s highlighted that the RMS activity did not display high degrees of variability over short chordal ranges, but it did show large and sudden changes in activity across the span. The facility to interrogate limited regions of the span, therefore allowed local effects to be isolated. Analysis of the data in this way has not yet been attempted, but this is discussed in relation to future work in Chapter 6.

4.2.5 Comparisons With Other Work

PV-WAVE code has been written to enable comparison of the results from static tests with results reported by other researchers. Zohar & Er-El[1] and Guglieri & Quagliotti[2] have reported results from static experiments carried out on a 60° and a 65° delta wing, each with sharp leading-edges, bevelled on the windward side and tested at Reynolds numbers of $Re = 0.5 \times 10^6$ and $Re = 1.75 \times 10^6$ respectively. Over-laid plots have been made of C_P against z/s using data from the current study ($Re = 1.5 \times 10^6$) and that extracted from the above reports, the data from the current study being

[1] Zohar & Er-El (1988)
[2] Guglieri & Quagliotti (1997)

carefully chosen so as to match as closely as possible the parameters (i.e. alpha and x/c position) plotted by the others.

The comparison of the data from the current study and that of the Zohar and Guglieri wings did not show a particularly good match across the range of results plotted. However, some results (Figure 4.11) showed that the magnitude and position of the peak negative C_P at comparable values of alpha and x/c position are of a similar order. Clearly, further investigation of the anomalies identified at the stage, is required.

4.2.6 Other Analysis Techniques

Greenwell & Wood[1] have derived a shape parameter for the vortex-induced upper surface pressure distribution on a delta wing from a simple two-dimensional potential flow model. In this model, the half-width of the suction peak is a function solely of the vortex height above the wing surface. PV-WAVE code has been written to calculate the non-dimensional half-width ($Z_{(0.5)}/s$) of the negative C_P suction peak previously plotted and described in sub-section 4.2.1. When calculated, $Z_{(0.5)}/s$ was plotted, as per Greenwell and Wood, for each value of alpha against x/c (Figure 4.12) and for each chord station against alpha (Figure 4.13).

At positive values of alpha, the plots of $Z_{(0.5)}/s$ v x/c showed a series of expansion 'bubbles' in the half-width trace which were seen to move towards the apex of the wing as alpha was increased. At $\alpha = 19.4835°$, (Figure 4.13) a narrowing of the half-width occurred between x/c = 0.6 and 0.65, followed by a rapid expansion until x/c = 0.85. As alpha was increased still further this rapid expansion was seen to occur at lower values of x/c until at $\alpha = 24.182°$, the expansion point reached x/c = 0.2, the forward limit of the plot. The plots of $Z_{(0.5)}/s$ v alpha closely follow the above results with a rapid expansion of the half-width occurring at $\alpha = 24.182°$ at chord station x/c = 0.2. For subsequent chord stations the expansion point occurs at earlier values of alpha until x/c = 0.65. Thereafter, the expansion point remains constant at $\alpha = 19.4835°$.

[1] Greenwell & Wood (1992)

Following on from the work described in sub-section 4.2.4, PV-WAVE code has been written to calculate the first derivative with respect to the non-dimensional chord of the maximum RMS pressure ($\partial(RMS_{max})/\partial(x/c)$). When calculated, $\partial(RMS_{max})/\partial(x/c)$ was plotted against x/c for a range of values of alpha. Initial analysis of these plots has suggested a possible relationship between the $\partial(RMS_{max})/\partial(x/c)$ trace and the RMS pressure field illustrated by the 2-D contour plots described in sub-section 4.2.2. Further detailed analysis of these plots is required and as such will be discussed in Chapter 6.

5. VALIDATION EXPERIMENTS

As part of the current study it is proposed to carry out a series of experiments using the smoke flow visualisation facility at Glasgow University. The purpose of these experiments are to act as an aid to, and to act as a validation tool for, the analysis of the results of the wind-tunnel tests carried out previously. The smoke flow visualisation experiments are to be carried out in the Reynolds number range of $5000 \leq Re \leq 40000$, using scaled down models of those described in Section 3.1. The justification for carrying out these tests at much lower Reynolds numbers and on scale models is based on the findings of Atta & Rockwell[1]. They reported that the position of vortex breakdown on a stationary wing did not change significantly over the Reynolds number range $2900 \leq Re \leq 13400$ and agreed well with other investigations up to $Re = 10^6$. The following chapter describes the progress of the work so far.

To carry out these experiments, two delta wing models have been specially designed and built at Glasgow. Each is a scaled down model of the wing previously described in this report in each of its two nose configurations. To make construction somewhat simpler, it was decided to build two complete wings rather than a single model with inter-changeable nose sections. Each is geometrically similar to its larger counterpart (c = 346.41mm, 2s = 400mm) with the space previously taken up by transducers being utilised as a plenum chamber to aid even smoke distribution. Smoke is to be passed into the model through a tube connected to a fitting in the centre of the windward surface. The smoke emerges through a slit, 0.2mm wide[2], located along the entire leading edge of the wing, 2.0mm below the leeward surface.

The lower surface of each model was manufactured from a solid aluminium block as per the larger wing. The plenum chamber was then routed and a series of 'smokeways' were machined 0.2mm deep, some parallel to the leading-edge and some perpendicular, together providing a path for the smoke from the plenum chamber to the leading-edge (Figure 5.1). A separate top plate, 2.0mm thick with a correctly-bevelled edge was then made and fitted to give the model it's nominal dimensions. A

[1] Atta & Rockwell (1990)
[2] As per Lowson (1991)

mounting and control linkage was then designed and manufactured to suit the smoke-tunnel dimensions and control motor mounting system. Details of the mounting and control system will be reported in a subsequent report as the design of the system has yet to be finalised.

Trials were carried out using the sharp-nosed model prior to the manufacture of its round-nosed counterpart to test the control linkage, smoke production, laser illumination and model control. It was clear that the control linkage suffered from play in the nose mounting bearings about the longitudinal axis and that the model had a tendency for excessive movement in the lateral plane about the forward mounting. The first problem was addressed by replacing the single forward mounting plain bearing with a pair of thrust bearings mounted back to back in the same housing. The second problem was thought to be due to the length of the rear struts which were designed to pass through the tunnel floor. This was remedied by mounting sliding bearings at tunnel floor level to reduce the bending moment on the struts, and replacing the original aluminium rear struts with similar stainless steel items designed to be used with the sliding bearings.

Over a range of flow velocities, smoke was seen to emanate from all ports along both leading-edges. Modifications were required to produce the smoke as a 'sheet' rather than a series of 'jets' as observed in the initial tests. This involved opening up the 'outer' smokeways from 10mm to 16mm (Figure 5.1). Subsequent trials showed that this modification provided improved smoke generation which was adequate for visualisation purposes. The modification was then incorporated in the design of the round-nosed model.

Trials using the smoke-tunnel's 0.5W Argon laser proved to be satisfactory, although problems were encountered in model control. It was clear that, due to the weight of the model and linkages, the stepper motor employed in the trials was not powerful enough. For subsequent tests, a more powerful a.c. servo-motor will be used. The motor will be controlled using position control via a PC configured for the purpose. The control programme was written using LABVIEW Version 3.1.

6. FUTURE WORK

The previous chapters have detailed the work carried out so far in pursuit of the aims and objectives of this project. The purpose of this chapter is to detail the planned work for the future.

The limited analysis of the Handley-Page data carried out so far has posed a series of questions regarding the behaviour of the delta wing studied in this project. For example, the analysis of the plots of $Z_{(0.5)}/s$ v x/c described in section 4.2.6 indicate a series of 'bubbles' in the $Z_{(0.5)}/s$ trace that move toward the apex of the wing as alpha is increased, culminating in a rapid increase in half-width at $\alpha = 19.5°$ and x/c = 0.65. Interpretation of this result using Greenwell & Woods analysis[1] would seem to suggest the hypothesis that vortex breakdown remains downstream of the trailing edge until $\alpha = 19.5°$, at which point it 'leaps' onto the wing at x/c = 0.65. This hypothesis would seem to have a certain amount of credibility as Wentz and Kohlman[2] have cited a similar phenomenon for wings with sweep angles of 55° or less at static values of alpha, and indeed, a very small number of researchers[3] investigating cases of wings with sweep angles of 63° or greater have also noted the same effect. However, on the negative side, the majority of investigators[4] recording results from static experiments on delta wings over a range of sweep angles including 60°, have all recorded the fact that vortex breakdown passes over the trailing-edge in a steady fashion.

The plots of RMS v z/s and the 2-D contour plots of RMS distribution described in section 4.2.2 indicate two ridges of high RMS activity; one at a point somewhat inboard of the corresponding C_P suction peak, and for certain values of x/c, a second smaller peak outboard of the C_P peak value. As yet, the reasons for this are not clear although it has been hypothesised that the larger peak of RMS activity may correspond to the primary vortex attachment line and the smaller peak may be related to either the secondary vortex separation or attachment lines.

---

[1] ibid.
[2] Wentz & Kohlman (1971)
[3] Elle (1960), McKernan et al (1988)
[4] Lawford & Beauchamp (1961), Lowson (1964), Hummel & Srinivasan (1966), Lee & Ho (1990) Panton (1990),

It is hoped to provide further clarification of these issues by conducting smoke visualisation experiments using the models described in Chapter 5, which will replicate the previous pressure measurement tests in terms of alpha ranges, ramp velocities and oscillation frequencies. It is proposed to build a collection of digitised photographic images of the flow from which it should be possible to determine the position of non-dimensional vortex height, lateral position and core width. In addition, the lines of flow attachment and separation and the vortex breakdown position over the entire alpha range will be examined.

In addition to the photographic images, it is proposed to observe the type of vortex breakdown that occurs over the models under both static and dynamic pitching conditions, and to study patterns in the corresponding pressure data that may indicate breakdown type.

The ultimate aim of the work is to establish a reliable method of vortex breakdown detection using static data which can be applied equally to the dynamic case. If this is successful, a general method for determining vortex breakdown on delta wings from high resolution pressure measurements will result.

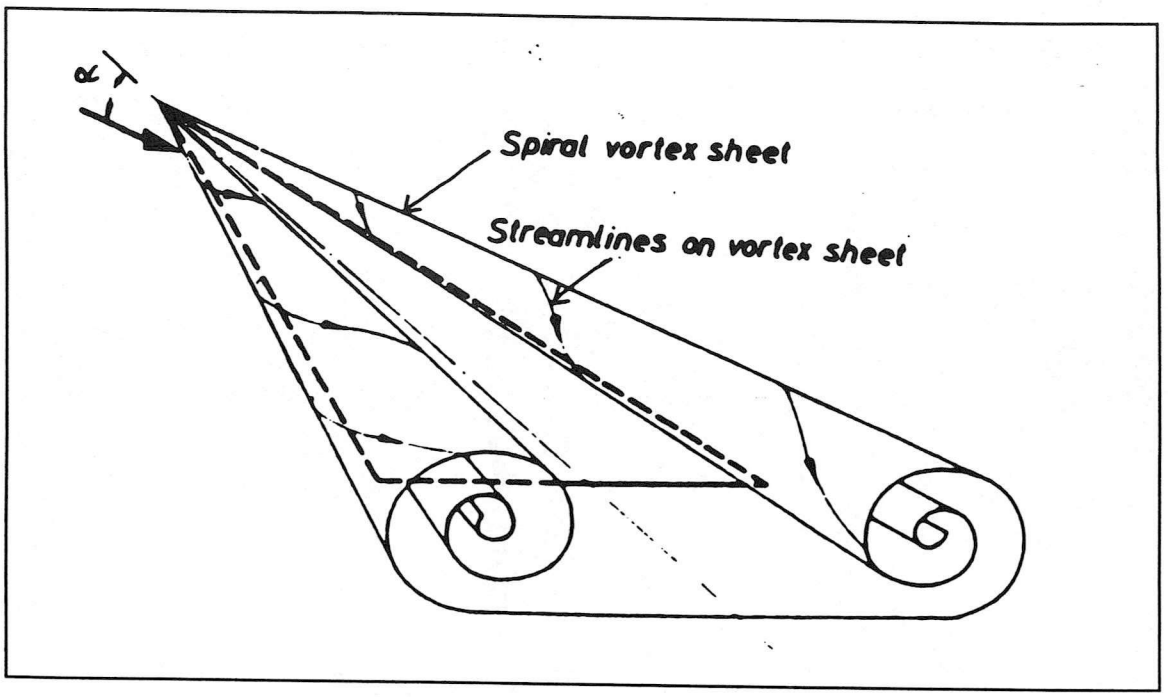

Figure 1.1 - Vortex Formation Over A Sharp-Edged Delta Wing[1]

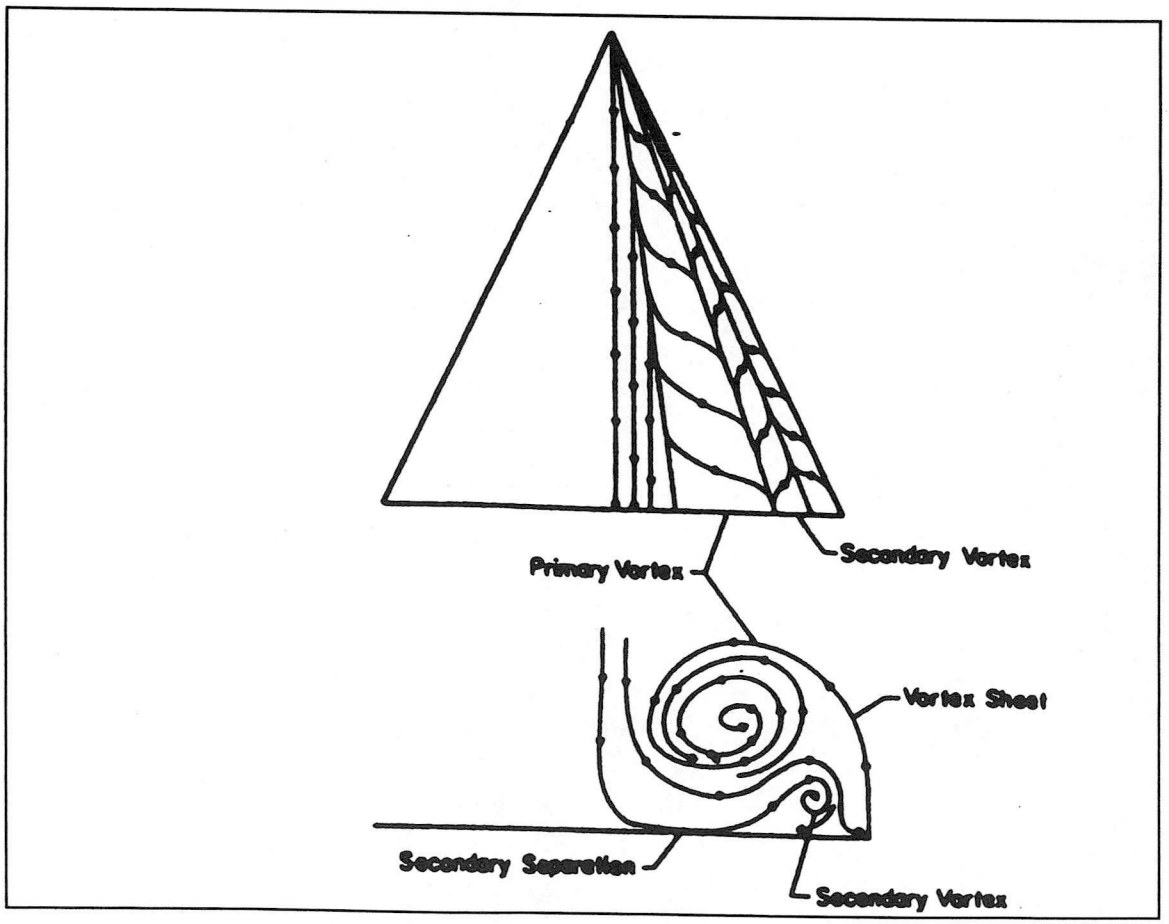

Figure 1.2 - Leading-Edge Vortex Flow Patterns[2]

[1] From Hummel & Srinivasan (1966)
[2] From Payne et al (1987)

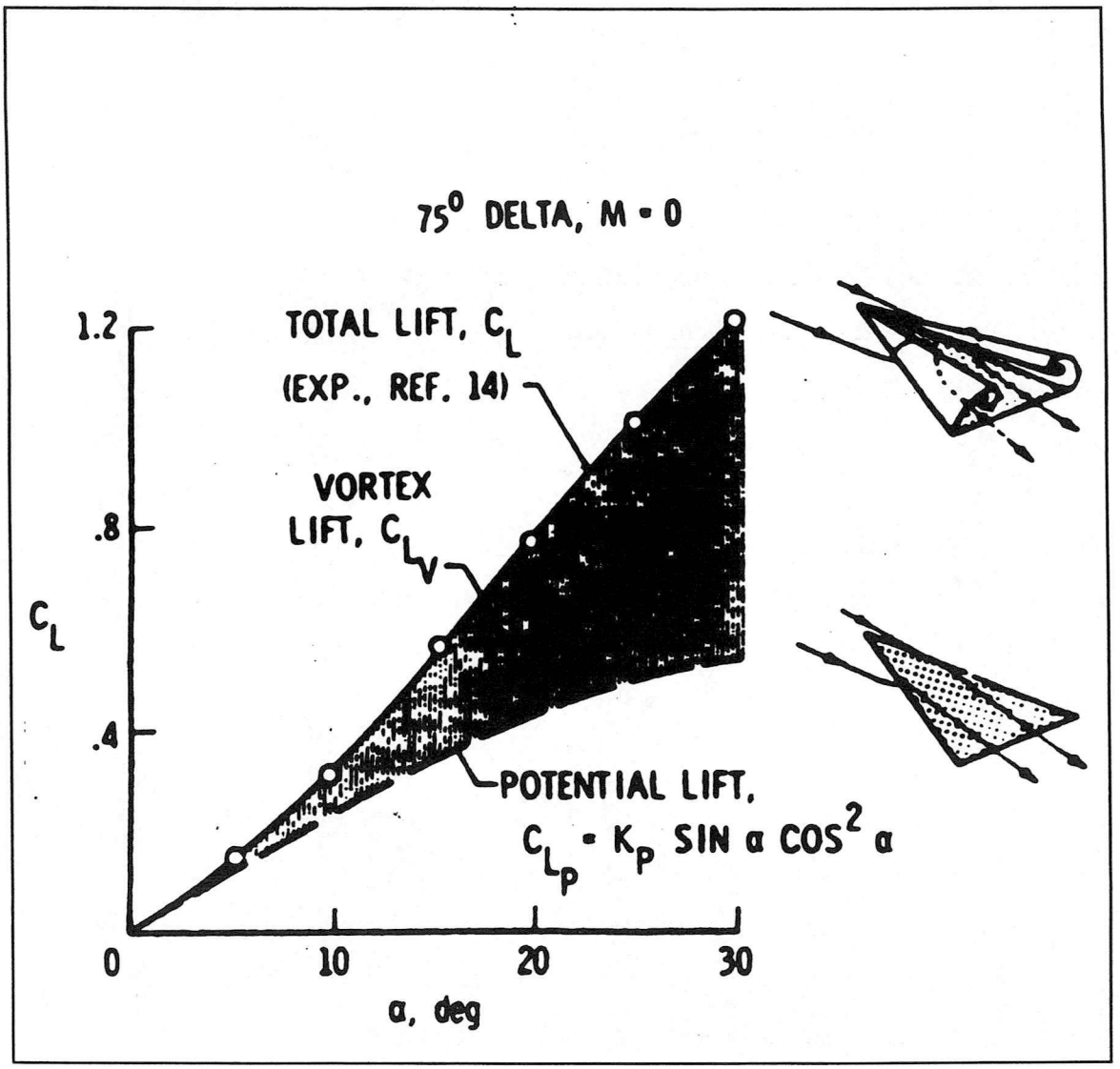

Figure 1.3 - Contribution Of Vortex Lift To The Total Lift Of A Delta Wing[1]

[1] From Polhamus (1971)

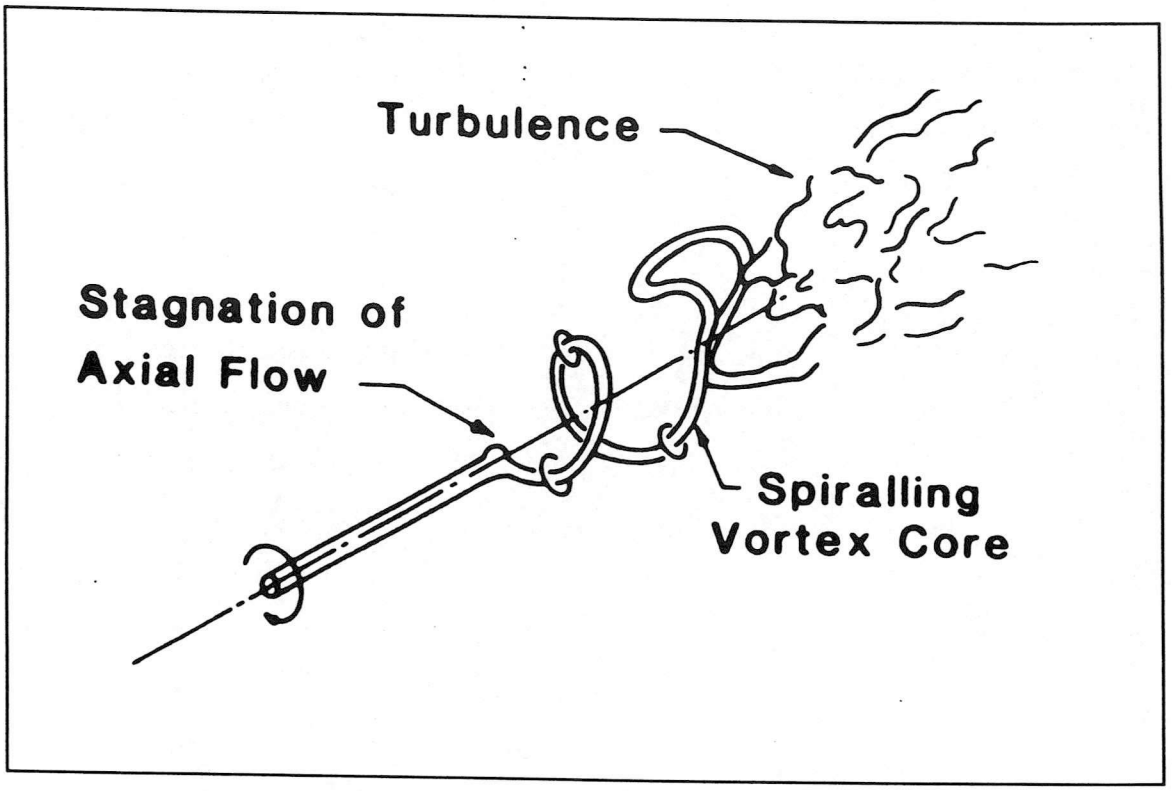

Figure 2.1 - Spiral (S-Type) Breakdown[1]

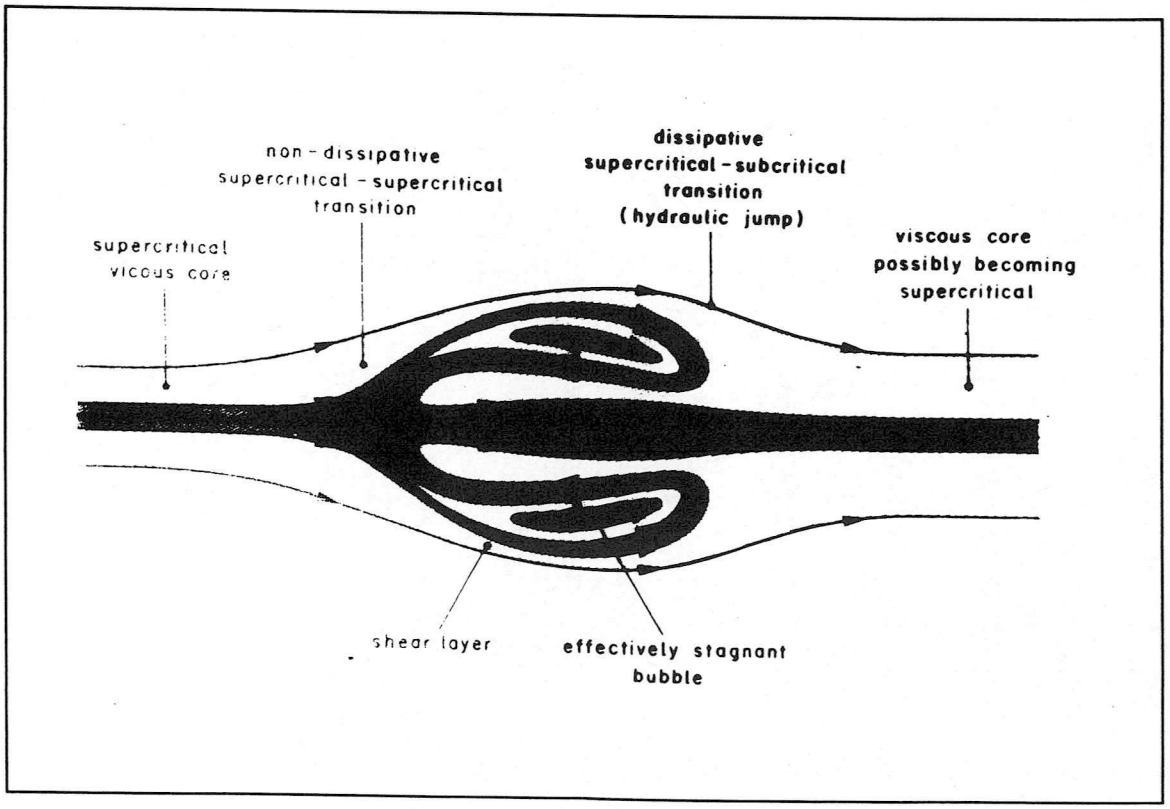

Figure 2.2 - Bubble (B-Type) Breakdown[2]

[1] From Payne et al (1986)
[2] From Escudier (1988)

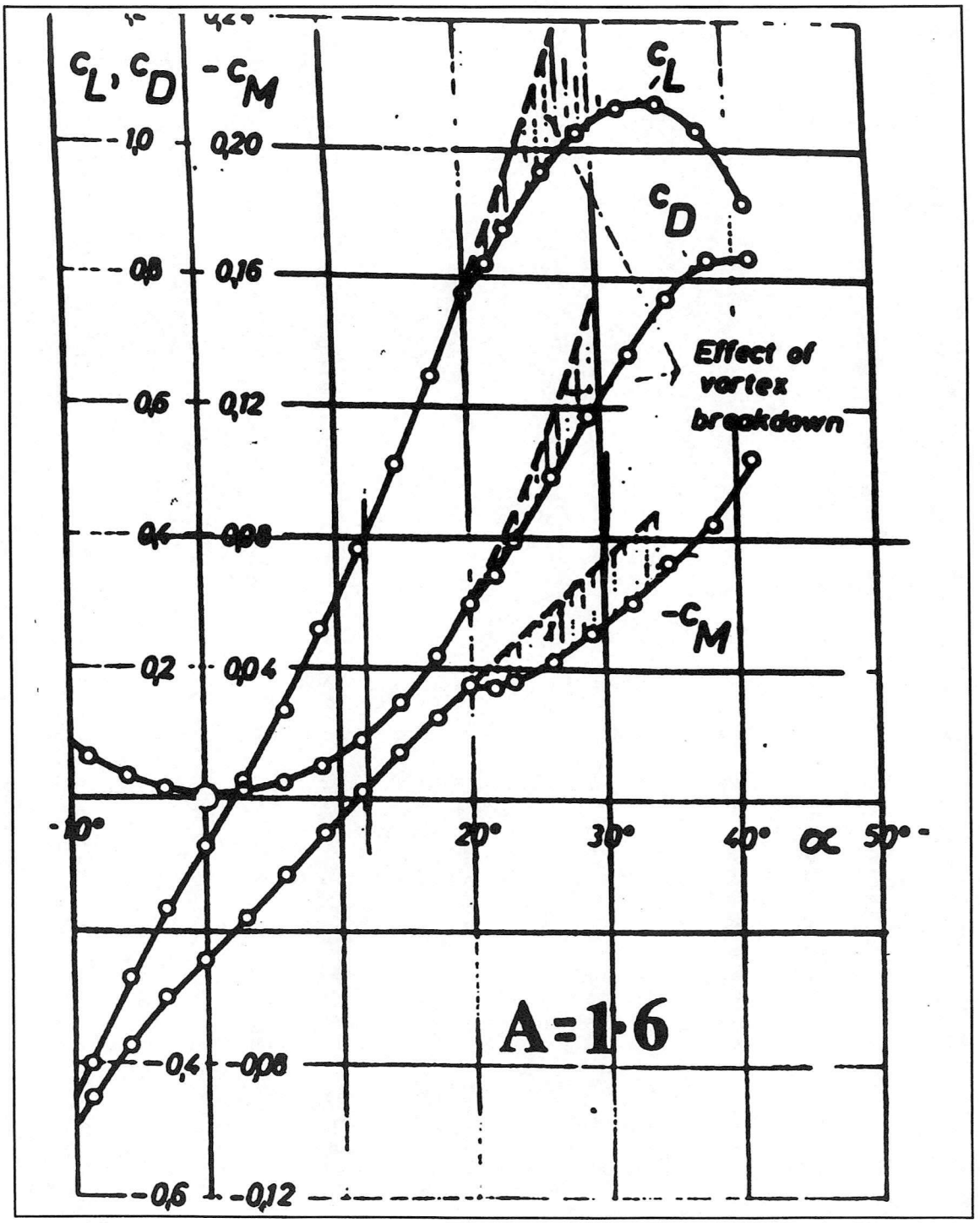

Figure 2.3 - Three-Component Measurements On A Delta Wing[1]

[1] From Hummel & Srinivasan (1966)

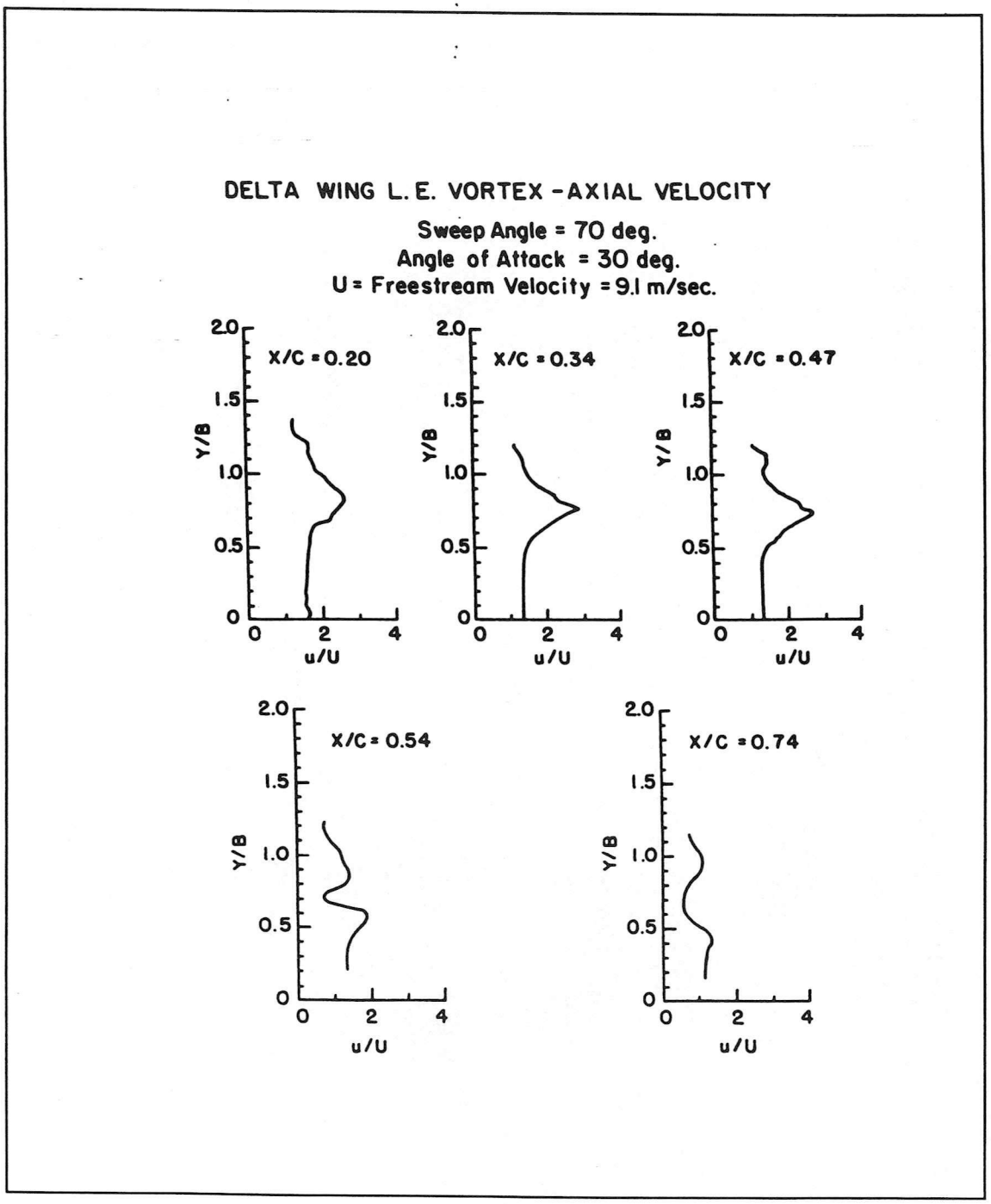

Figure 2.4 - LDA Measurements: Axial Velocity Profiles[1]

[1] From Payne et al (1986)

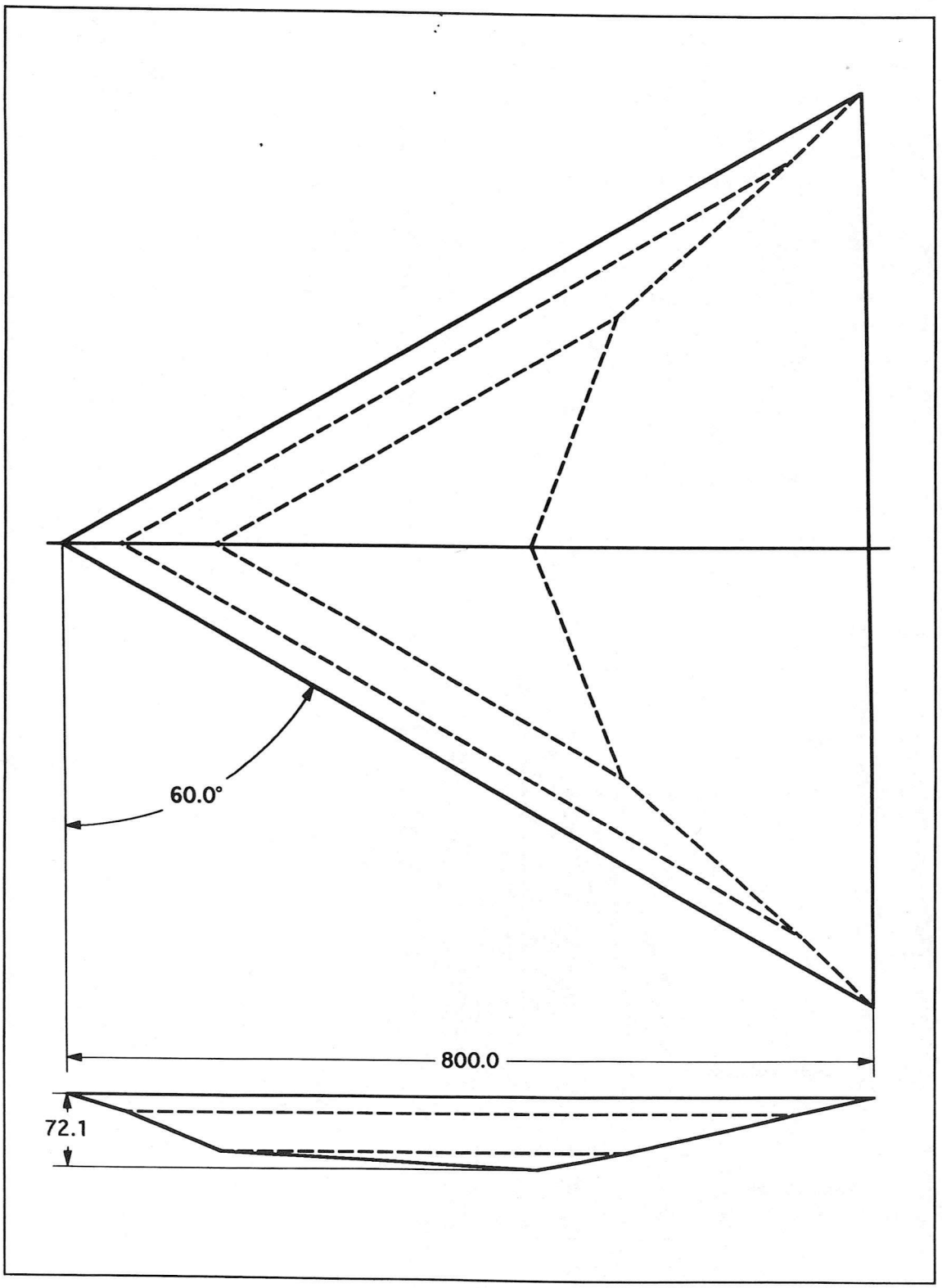

Figure 3.1 - The Handley-Page Model

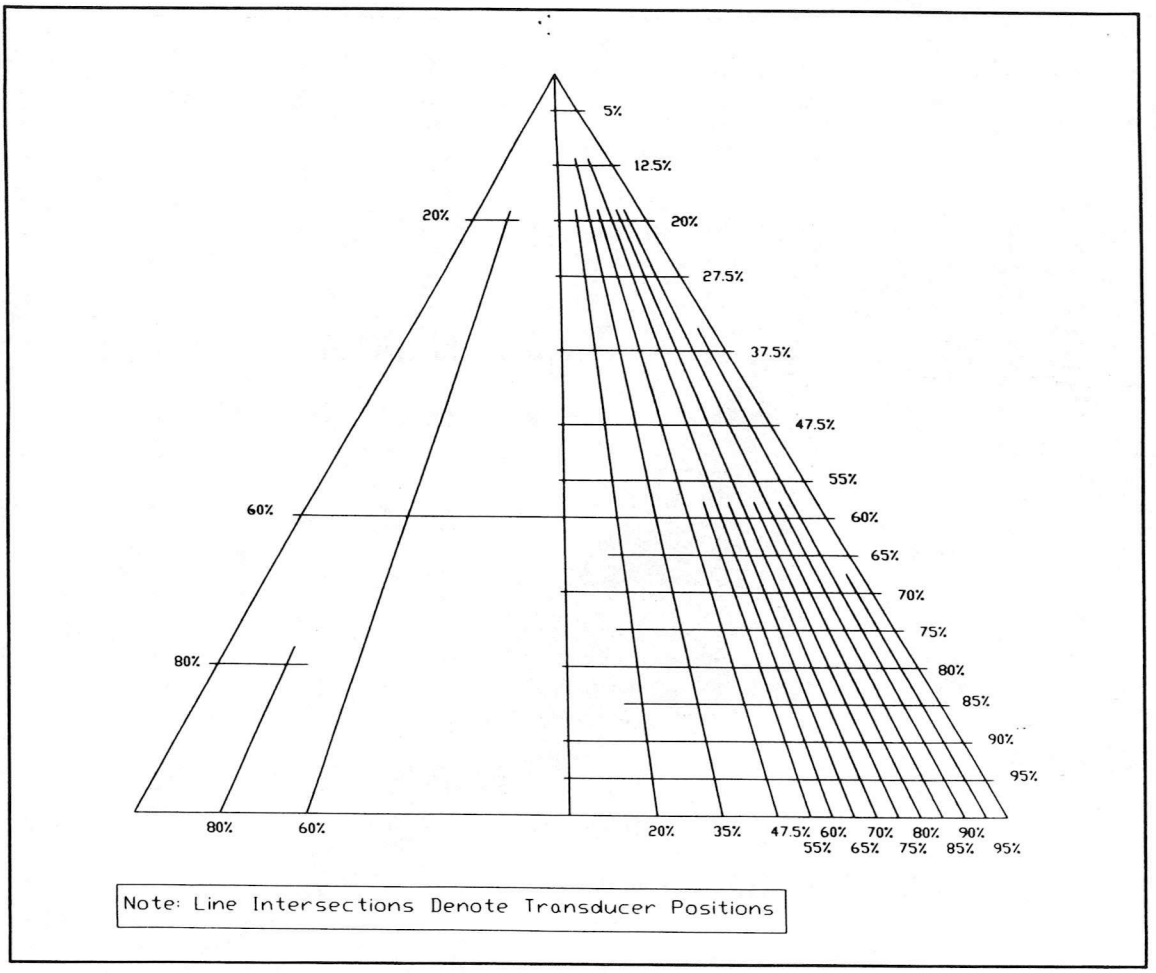

Figure 3.2 - Leeward Surface Transducer Positions

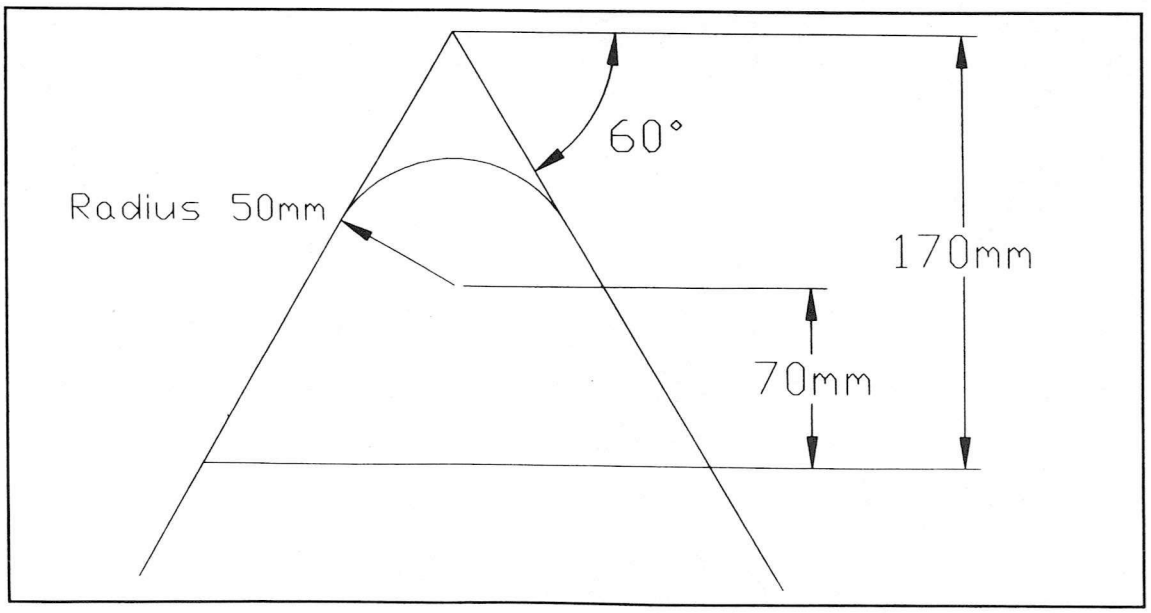

Figure 3.3 - Details Of The Round-Nosed Section

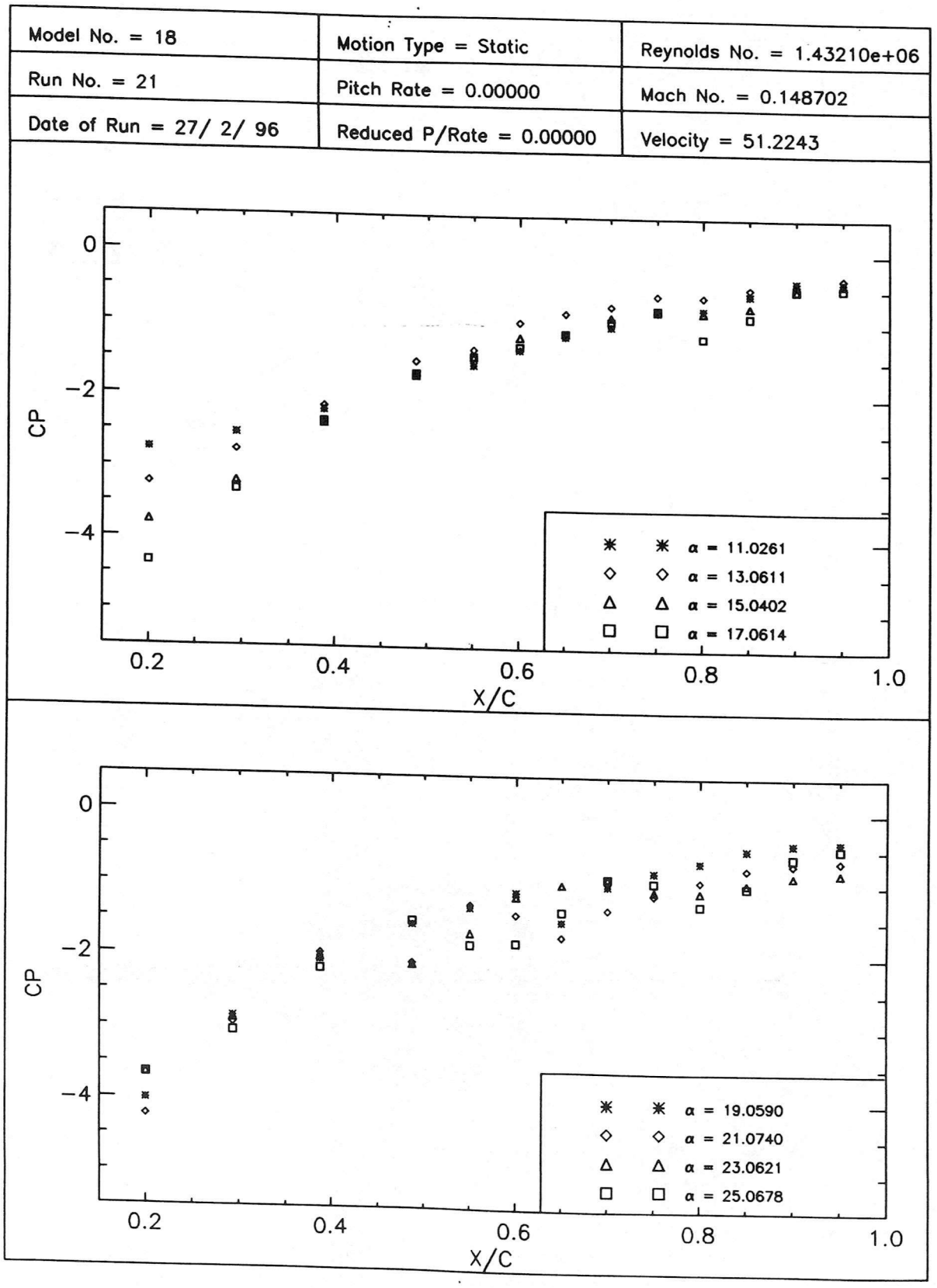

Cp v X/C at span station 9

Figure 4.1 - C_P v x/c (Version 1)

Model No. = 18	Motion Type = Static	Reynolds No. = 1.43210e+06
Run No. = 21	Pitch Rate = 0.00000	Mach No. = 0.148702
Date of Run = 27/ 2/ 96	Reduced P/Rate = 0.00000	Velocity = 51.2243

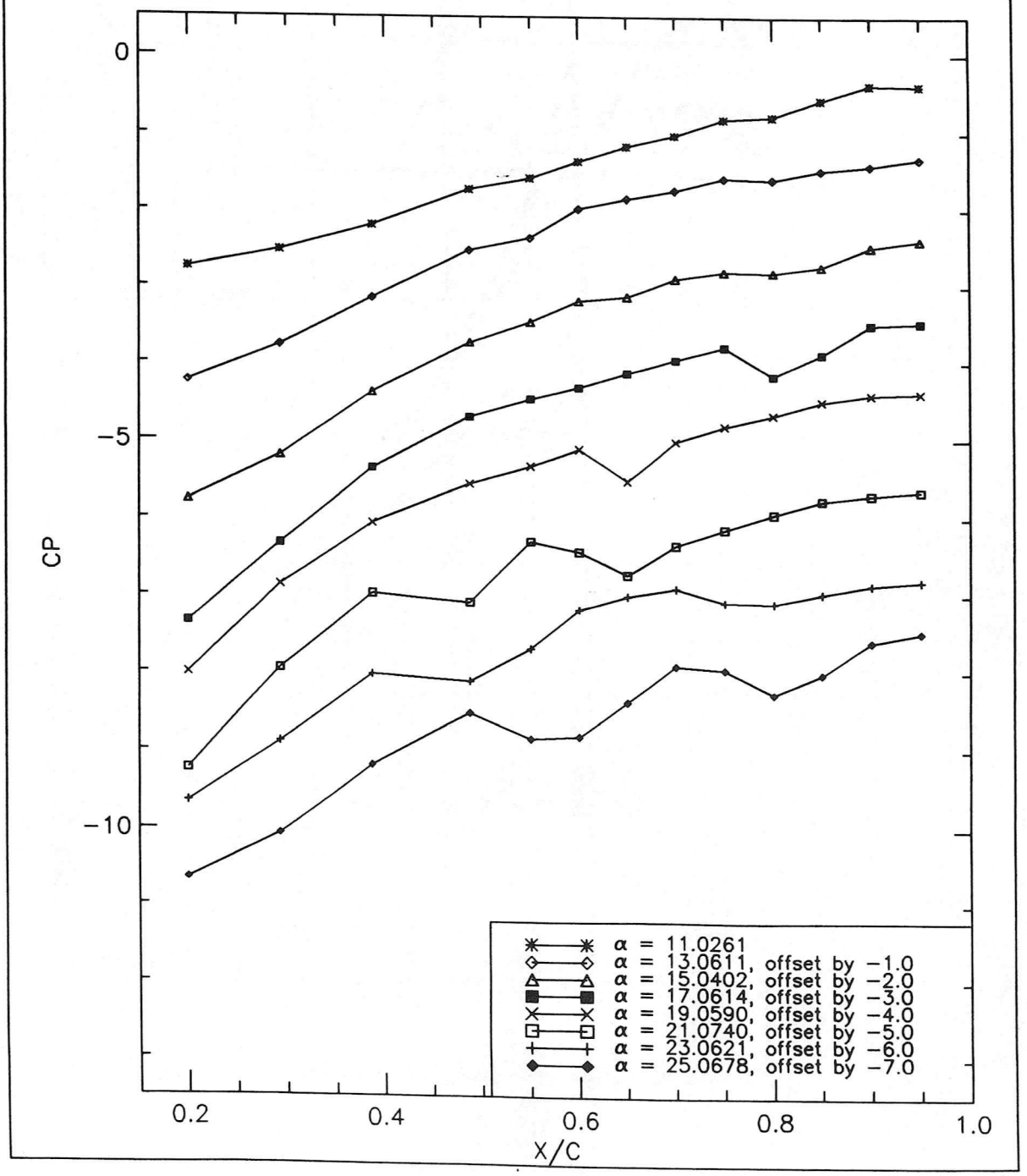

CP v X/C at span station 9

Figure 4.2 - C_P v x/c (Version 2)

Model No. = 18	Motion Type = Static	Reynolds No. = 1.43210e+06
Run No. = 21	. Pitch Rate = 0.00000	Mach No. = 0.148702
Date of Run = 27/ 2/ 96	Reduced P/Rate = 0.00000	Velocity = 51.2243

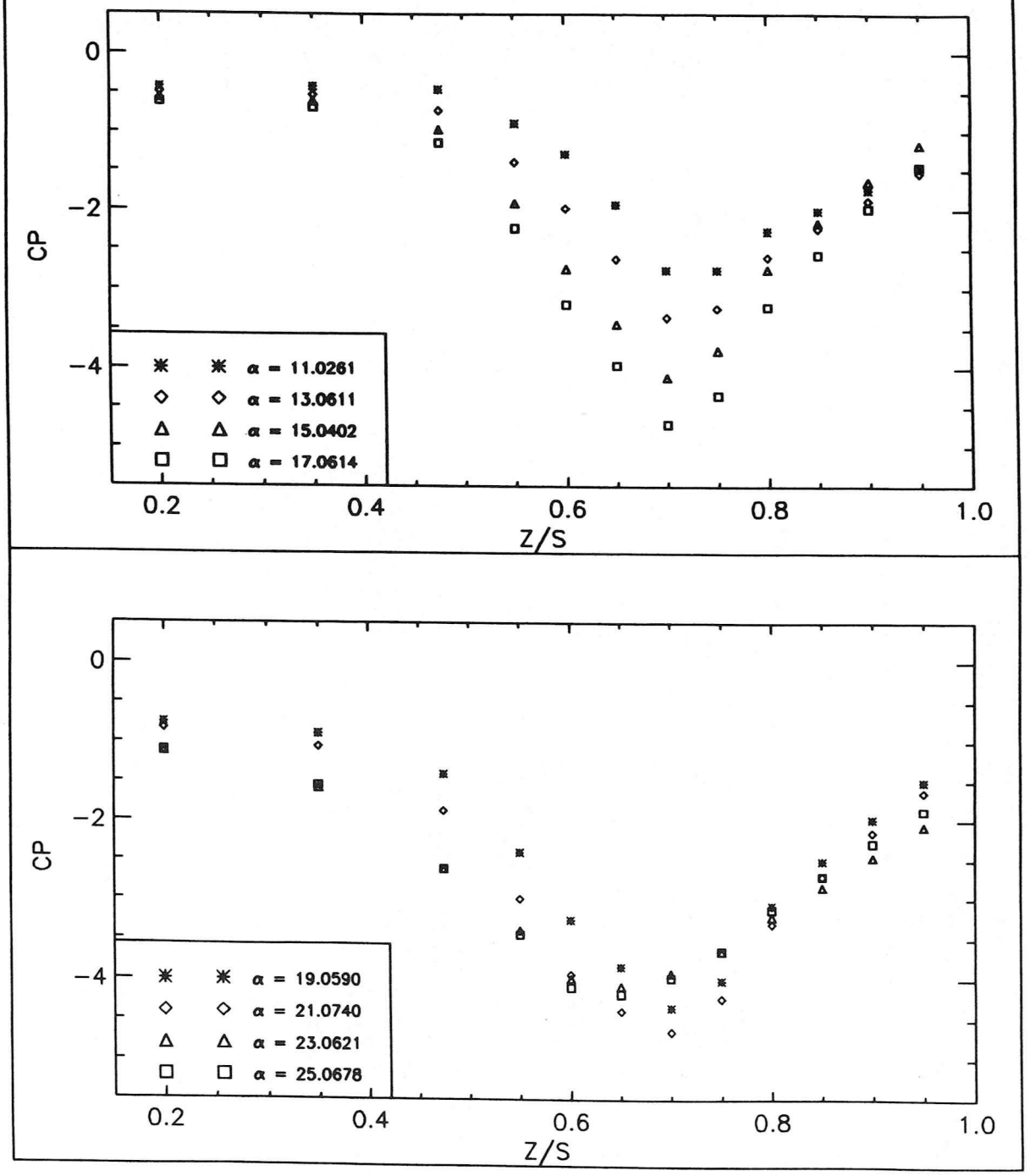

Cp v Z/S at chord station 4

Figure 4.3 - C_P v z/s (Version 1)

Model No. = 18	Motion Type = Static	Reynolds No. = 1.43210e+06
Run No. = 21	Pitch Rate = 0.00000	Mach No. = 0.148702
Date of Run = 27/ 2/ 96	Reduced P/Rate = 0.00000	Velocity = 51.2243

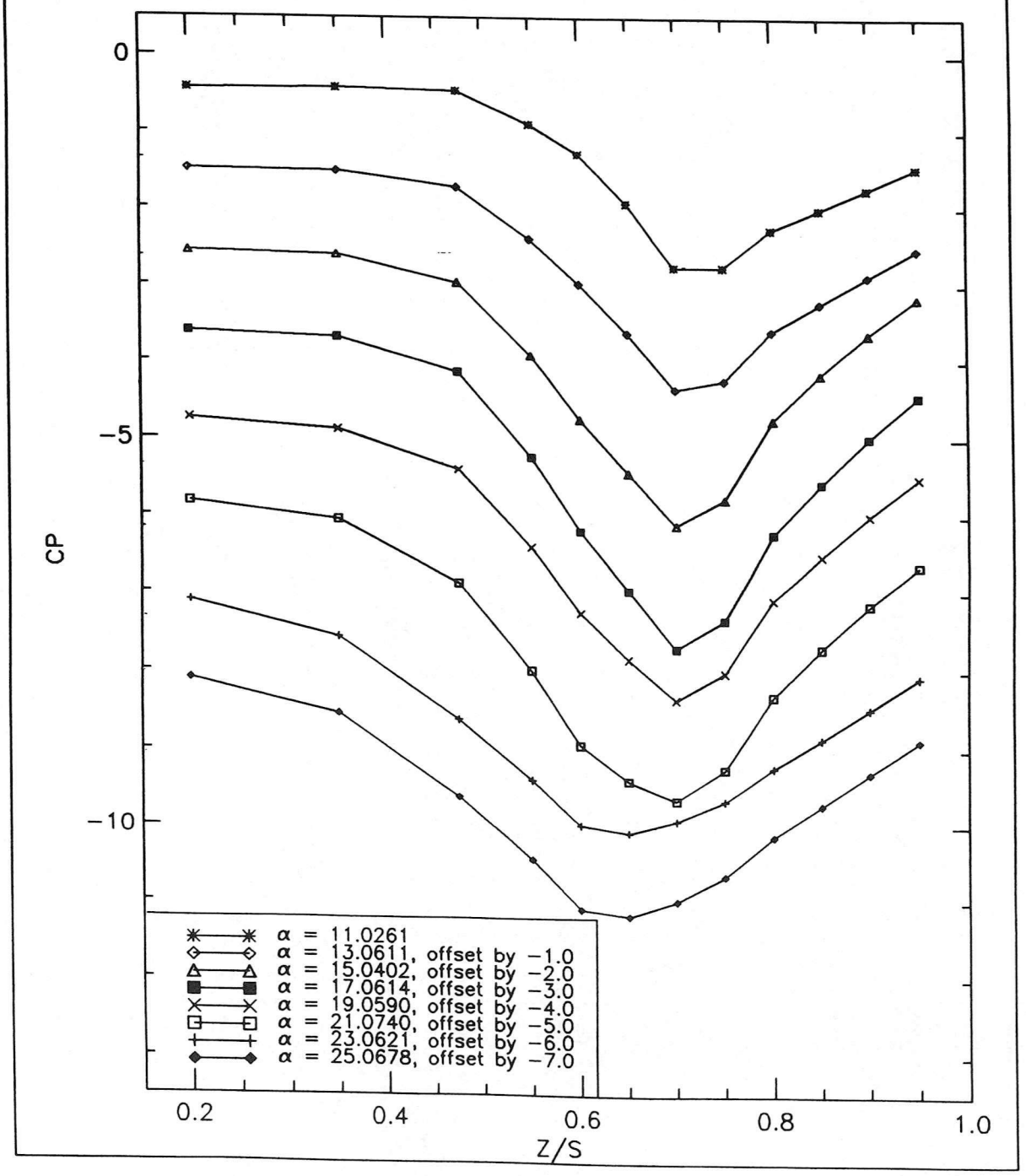

CP v Z/S at chord station 4

Figure 4.4 - C_P v z/s (Version 2)

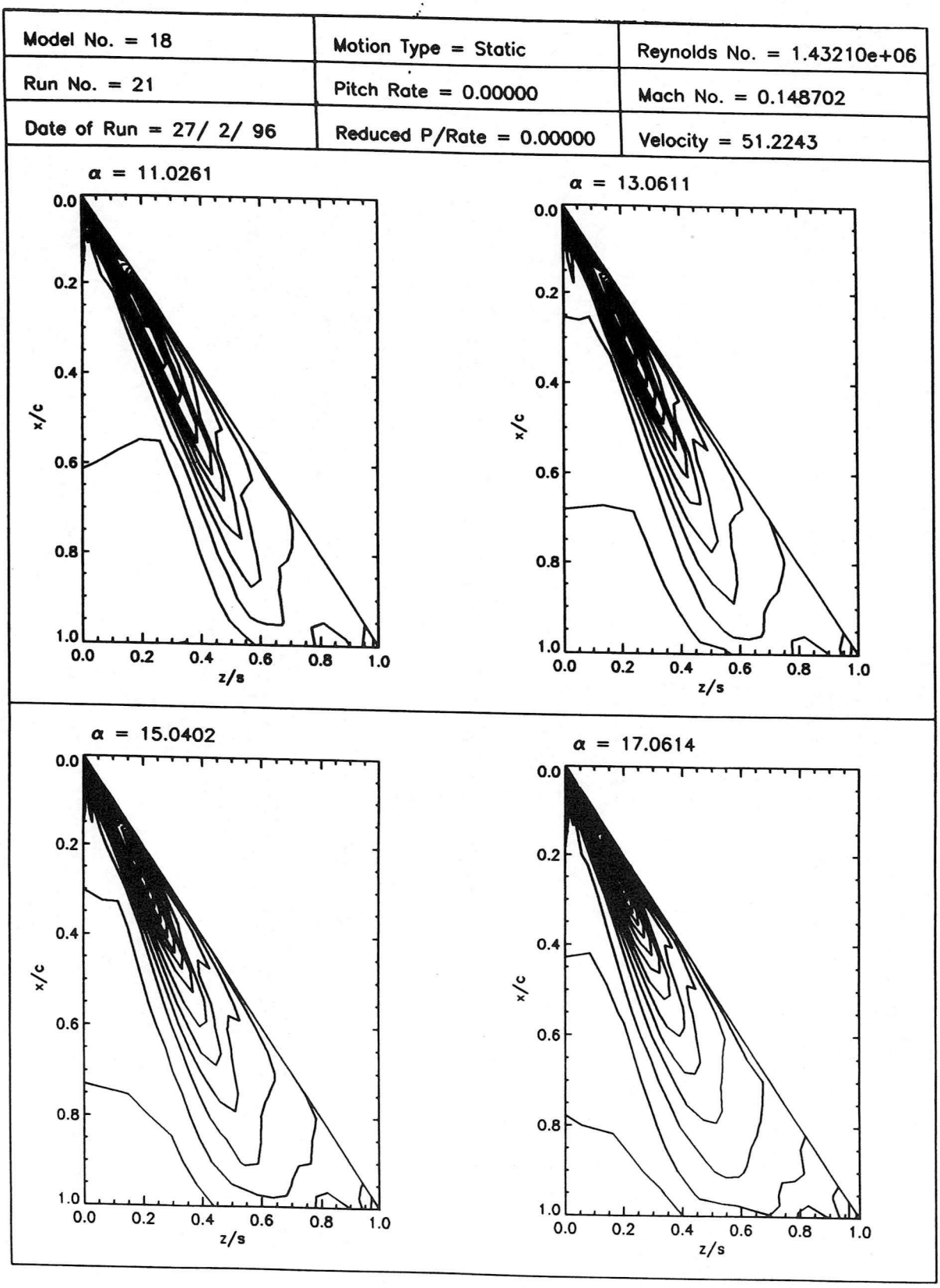

Cp Contour Distribution

Figure 4.5 - C_P 2-D Contour Plot

Model No. = 18	Motion Type = Static	Reynolds No. = 1.43210e+06
Run No. = 21	Pitch Rate = 0.00000	Mach No. = 0.148702
Date of Run = 27/ 2/ 96	Reduced P/Rate = 0.00000	Velocity = 51.2243

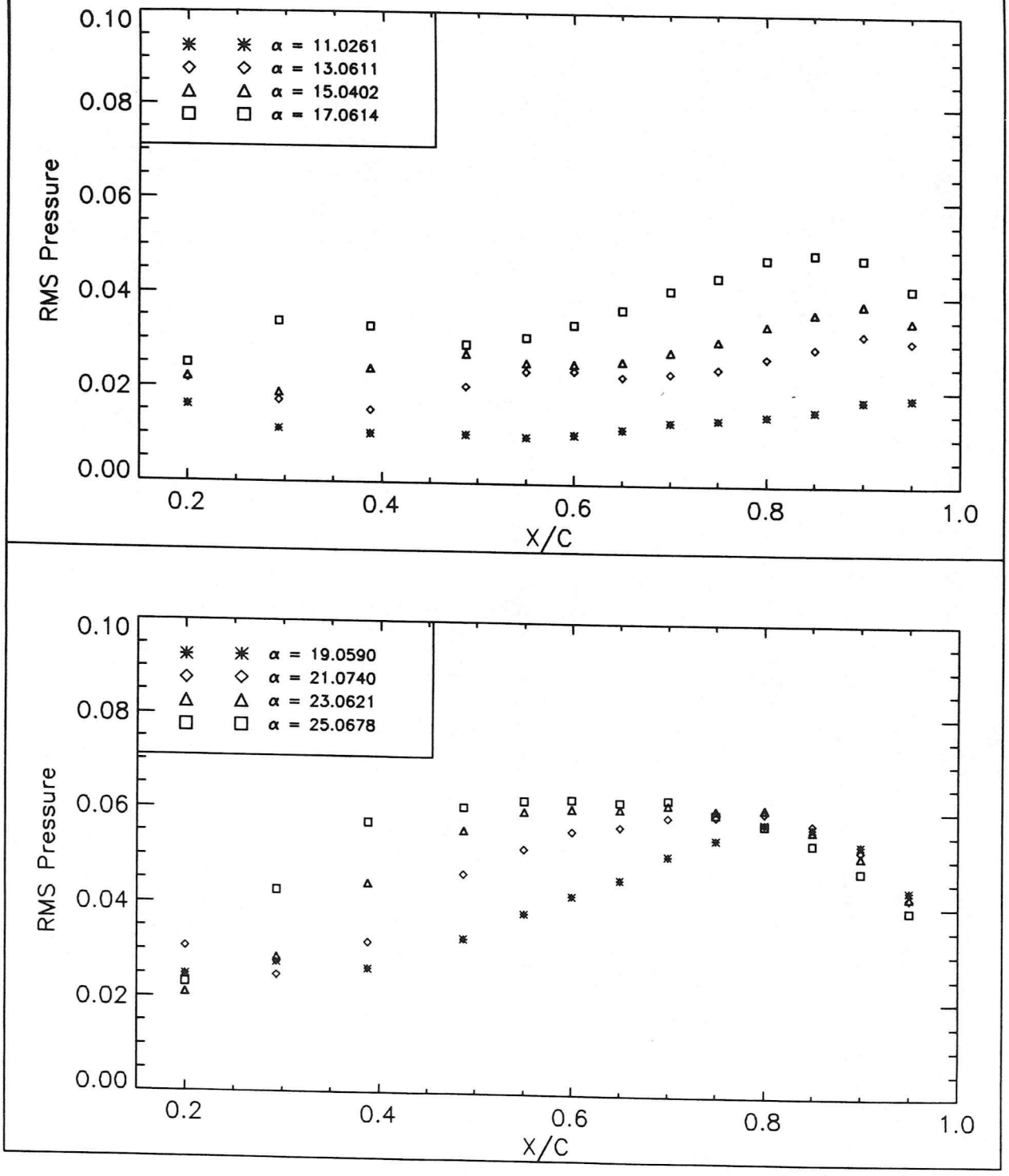

RMS Pressure v X/C at span station 4

Figure 4.6 - RMS v x/c

Model No. = 18	Motion Type = Static	Reynolds No. = 1.43210e+06
Run No. = 21	Pitch Rate = 0.00000	Mach No. = 0.148702
Date of Run = 27/ 2/ 96	Reduced P/Rate = 0.00000	Velocity = 51.2243

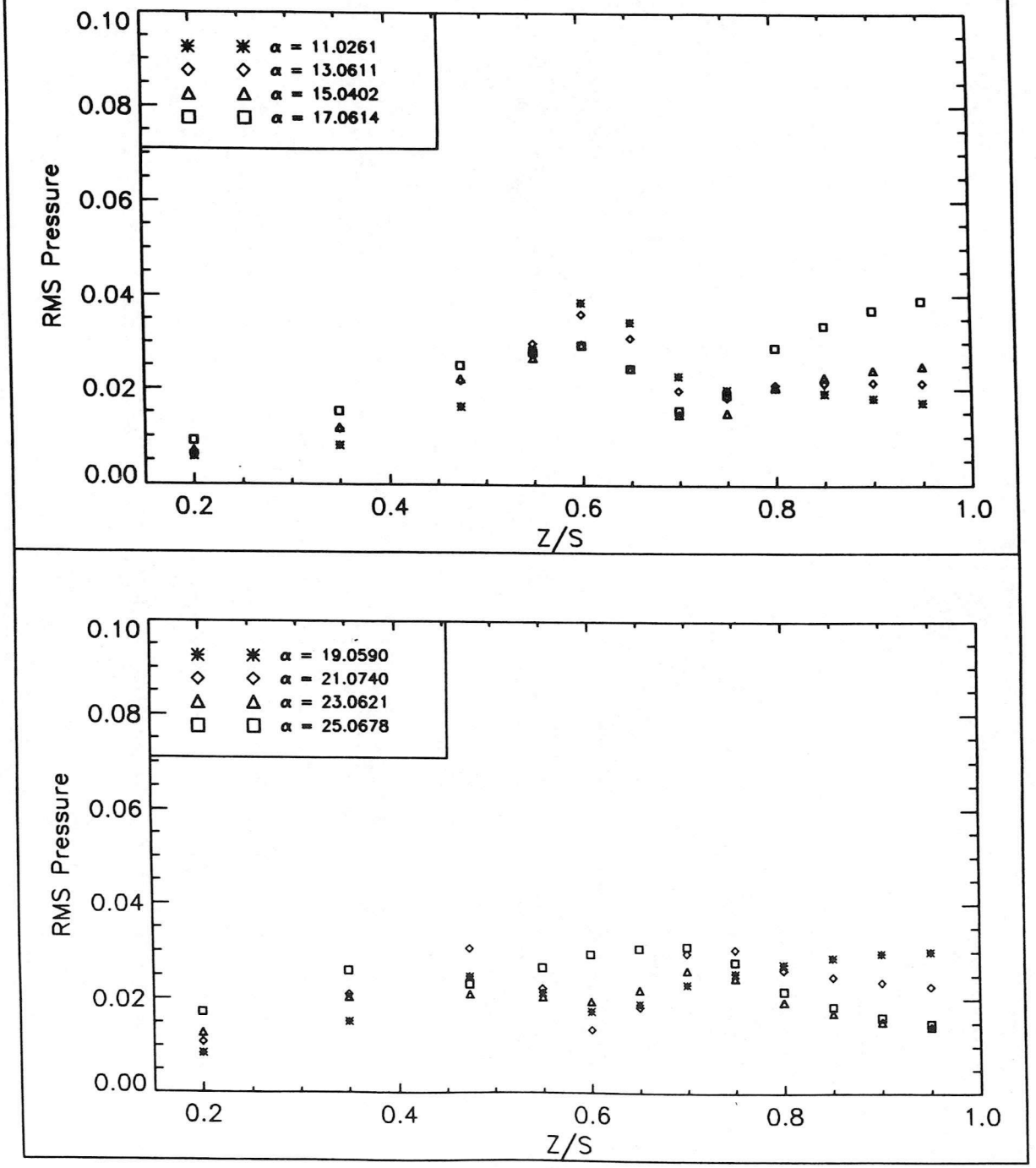

RMS Pressure v Z/S at chord station 4

Figure 4.7 - RMS v z/s

Model No. = 18	Motion Type = Static	Reynolds No. = 1.43210e+06
Run No. = 21	Pitch Rate = 0.00000	Mach No. = 0.148702
Date of Run = 27/ 2/ 96	Reduced P/Rate = 0.00000	Velocity = 51.2243

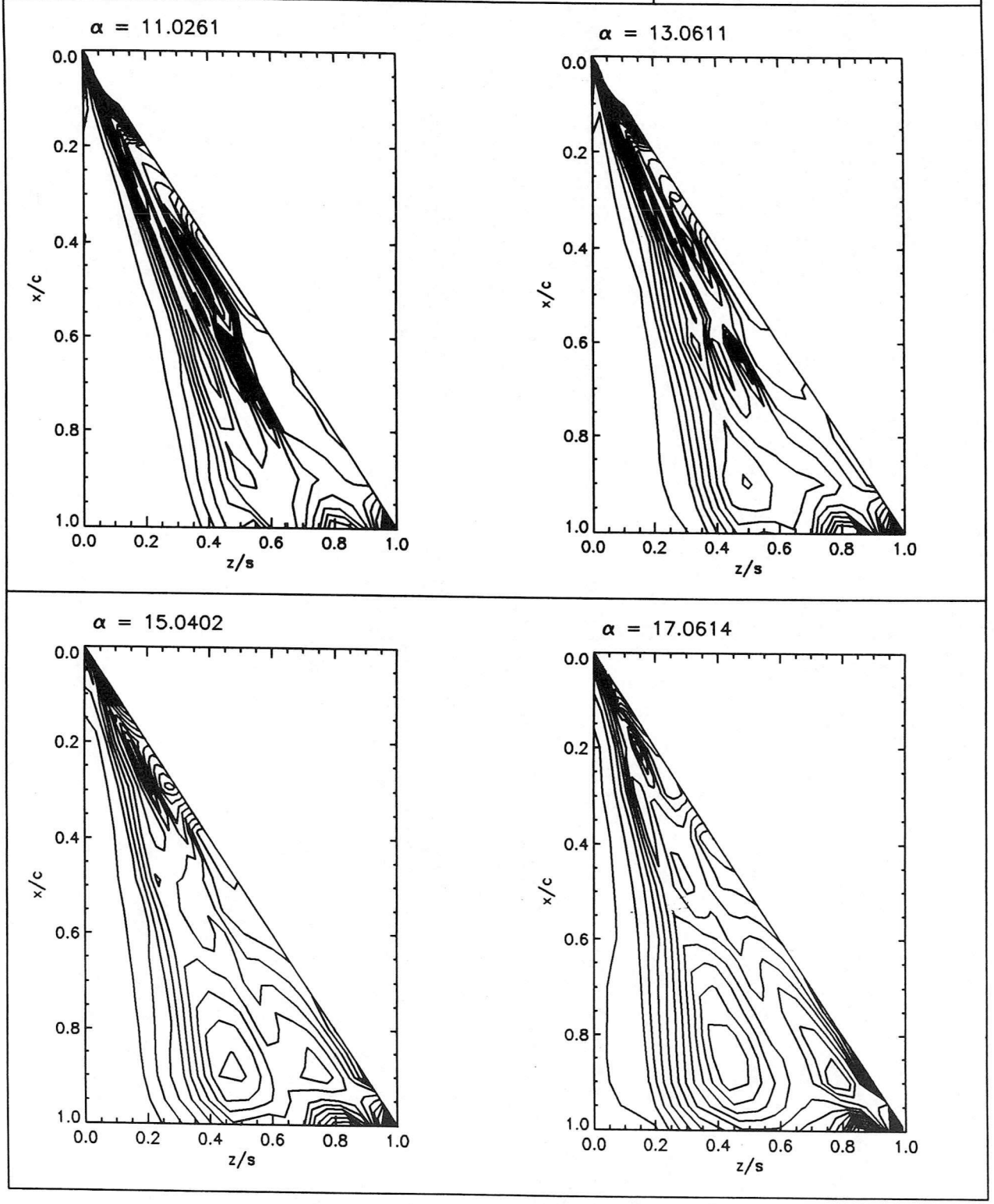

RMS Pressure Contour Distribution

Figure 4.8 - RMS 2-D Contour Plot

Model No. = 18	Motion Type = Static	Reynolds No. = 1.43210e+06
Run No. = 21	Pitch Rate = 0.00000	Mach No. = 0.148702
Date of Run = 27/ 2/ 96	Reduced P/Rate = 0.00000	Velocity = 51.2243

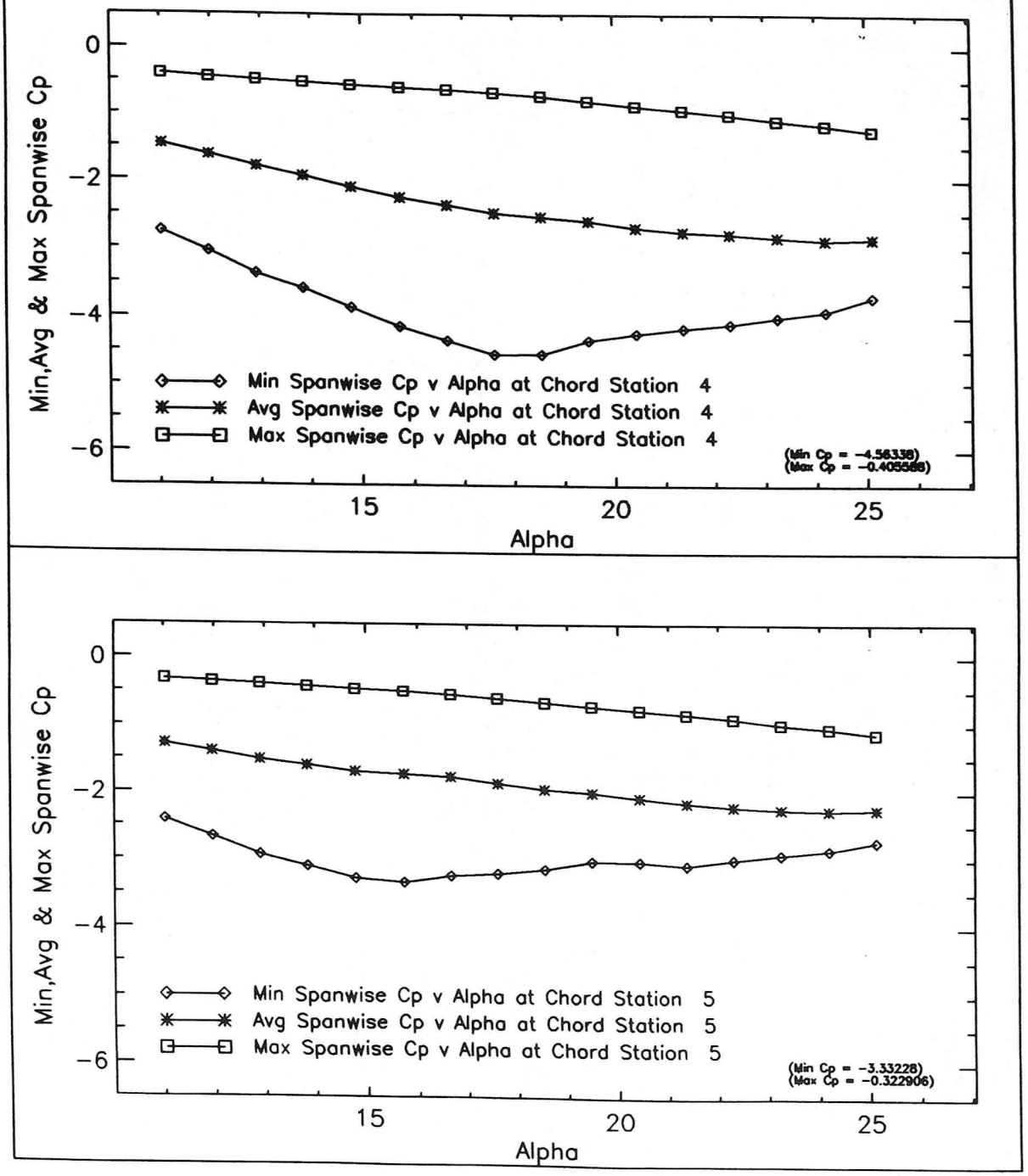

Min,Avg & Max Spanwise Cp v Alpha

Figure 4.9 - Min, Max & Average C_P v Alpha

Model No. = 18	Motion Type = Static	Reynolds No. = 1.43210e+06
Run No. = 21	Pitch Rate = 0.00000	Mach No. = 0.148702
Date of Run = 27/ 2/ 96	Reduced P/Rate = 0.00000	Velocity = 51.2243

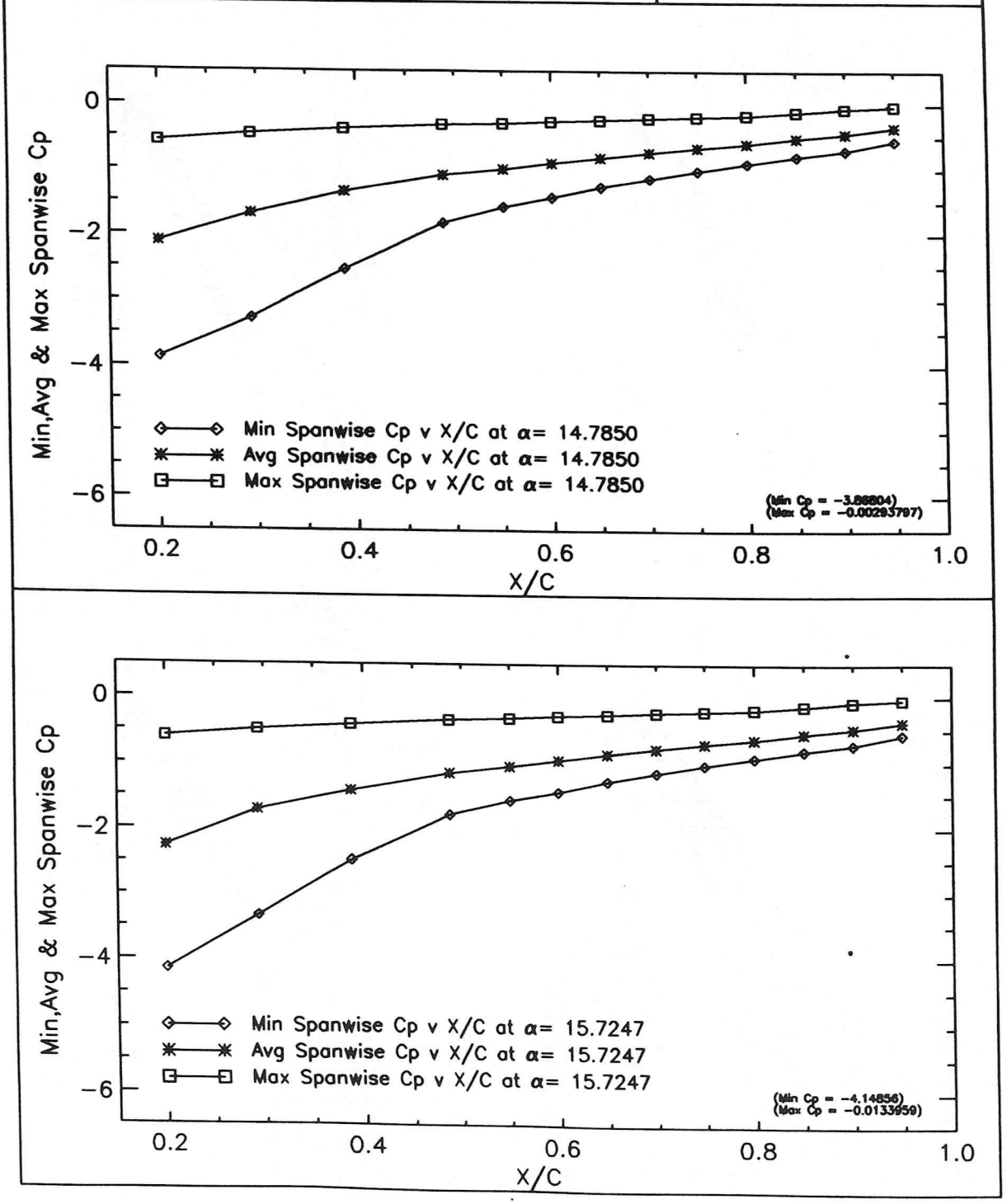

Min,Avg & Max Spanwise Cp v X/C

Figure 4.10 - Min, Max & Average C_P v x/c

Model No. = 18	Motion Type = Static	Reynolds No. = 1.43210e+06
Run No. = 21	Pitch Rate = 0.00000	Mach No. = 0.148702
Date of Run = 27/ 2/ 96	Reduced P/Rate = 0.00000	Velocity = 51.2243

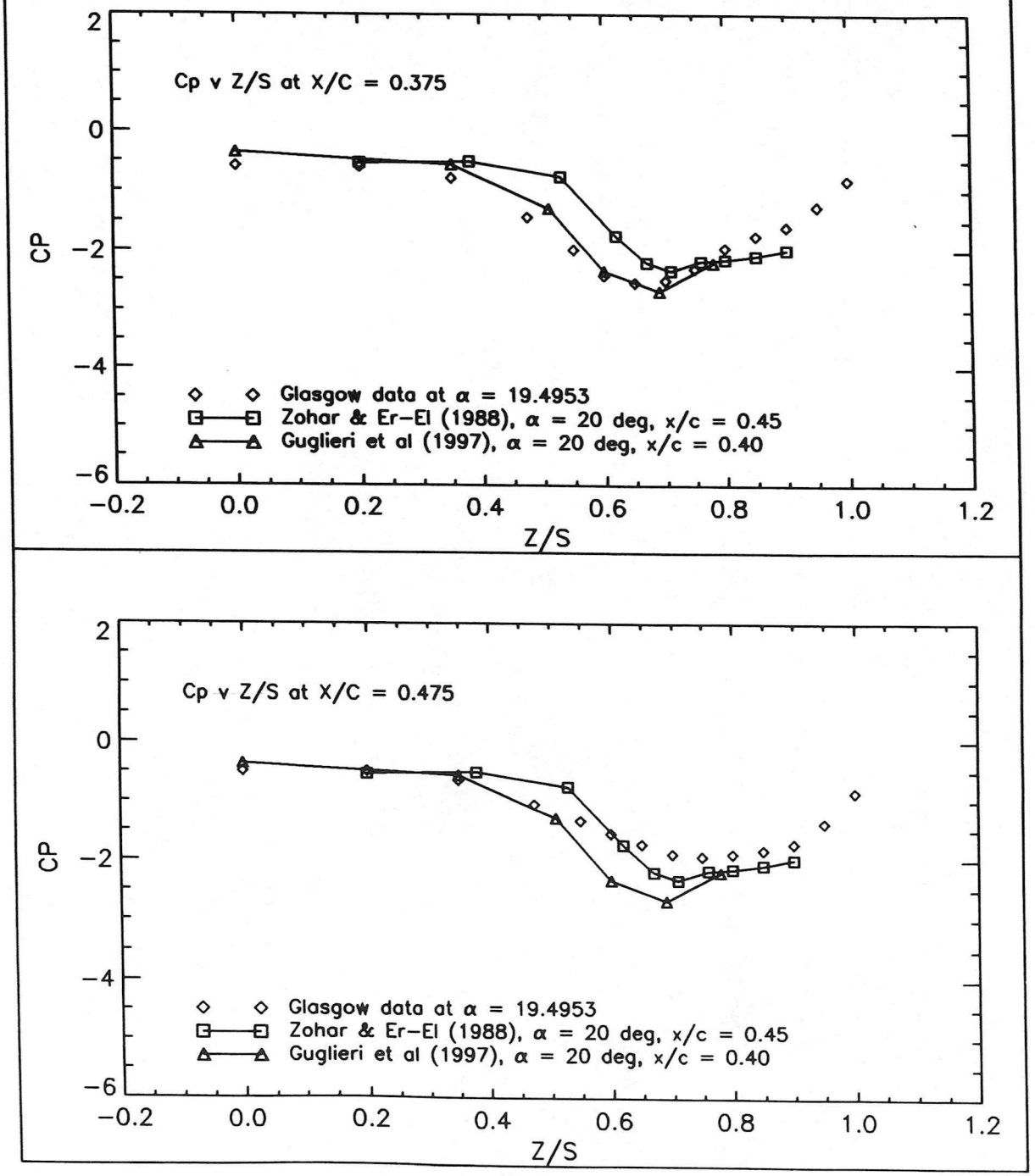

Comparison of Cp v Z/S

Figure 4.11 - Comparison Of Results (C_P v z/s)

Model No. = 18	Motion Type = Static	Reynolds No. = 1.43210e+06
Run No. = 21	Pitch Rate = 0.00000	Mach No. = 0.148702
Date of Run = 27/ 2/ 96	Reduced P/Rate = 0.00000	Velocity = 51.2243

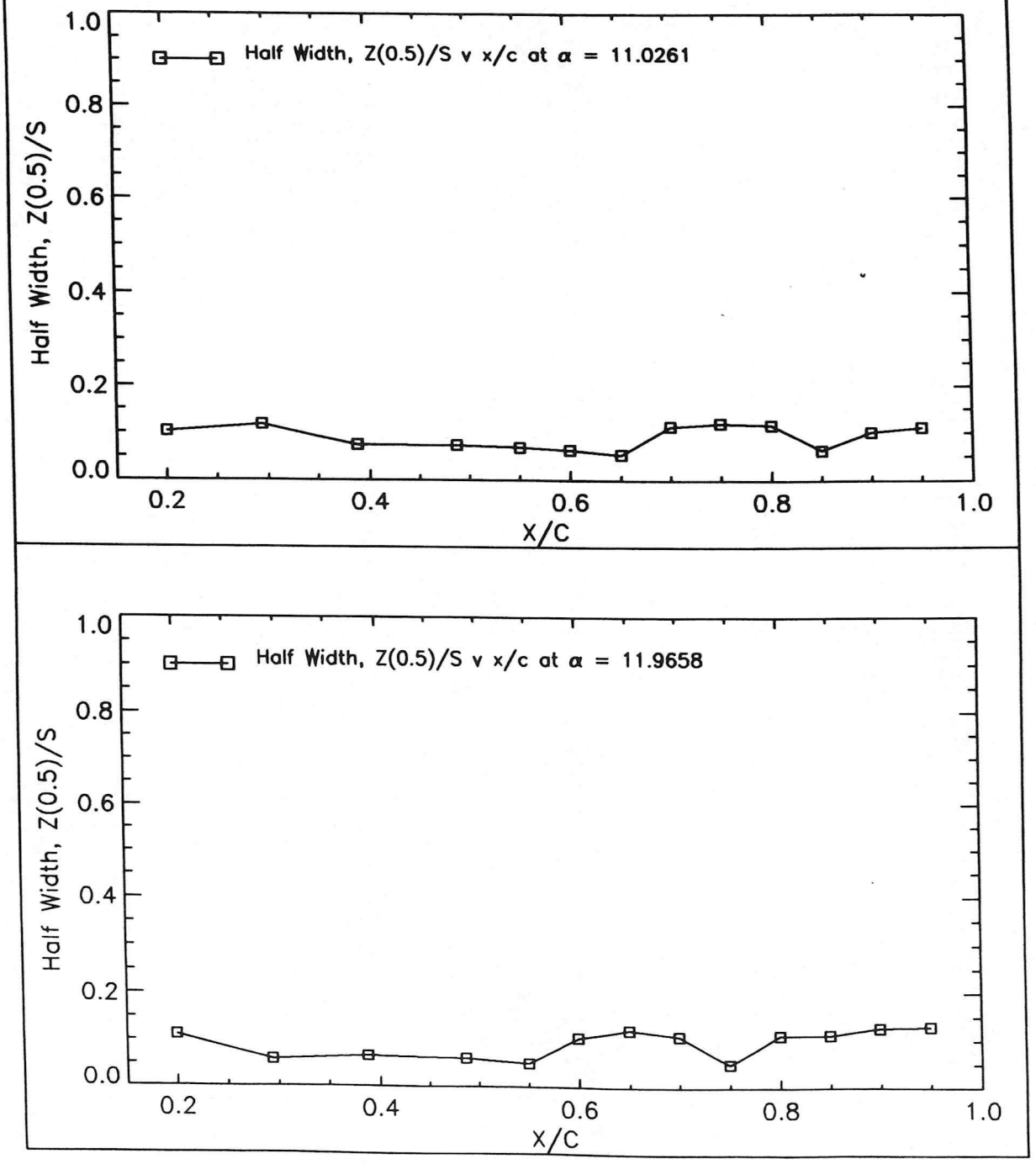

Half Width, Z(0.5)/S v X/C

Figure 4.12 - $Z_{(0.5)}/s$ v x/c ($\alpha = 11.0261°$)

Model No. = 18	Motion Type = Static	Reynolds No. = 1.43210e+06
Run No. = 21	Pitch Rate = 0.00000	Mach No. = 0.148702
Date of Run = 27/ 2/ 96	Reduced P/Rate = 0.00000	Velocity = 51.2243

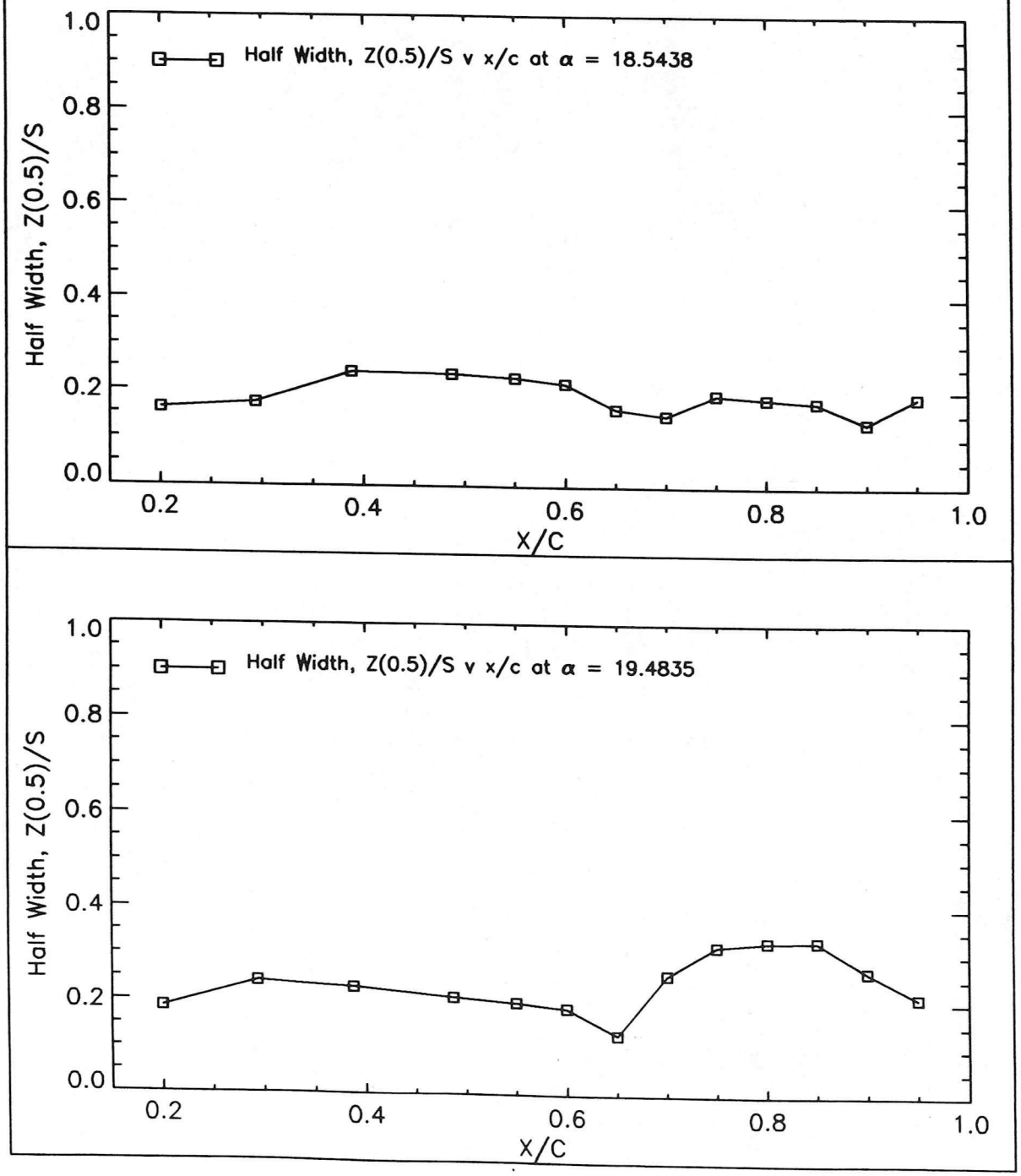

Half Width, Z(0.5)/S v X/C

Figure 4.13 - $Z_{(0.5)}$/s v x/c ($\alpha = 19.4835°$)

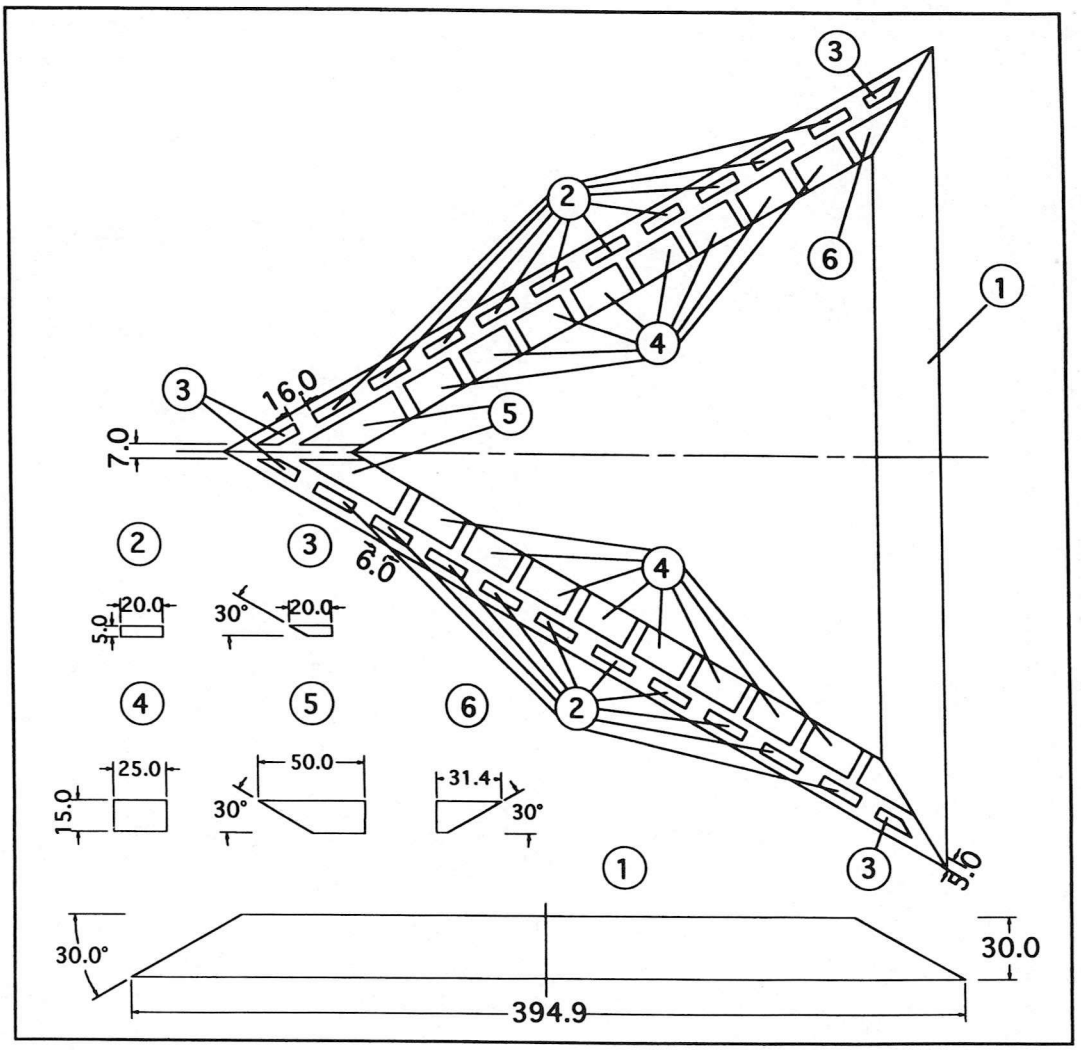

Figure 5.1 - Details Of Visualisation Model Smoke Delivery

APPENDIX A - Summary Of Previous Experimental Work

Category	Effect of...	Who	Date
Wing parameters	aspect ratio (constant sweep)	Lambourne & Bryer	1961
	aspect ratio (variable sweep)	Peckham & Atkinson	1957
	leading-edge shape	Kegelmann & Roos	1989
	camber	Weinberg	1992
	pitch axis location	Greenwell & Wood	1994
	trailing-edge geometry	Lee & Ho	1990
	apex geometry	Panton	1990
	wing thickness	Lowson & Riley	1995
Tunnel parameters	external pressure gradient	Gursul & Ho	1993
	tunnel interference	Berndt	1957
	ground proximity	Weinberg	1992
	free stream disturbances	Lee & Ho	1990
Test parameters	Reynolds number	Lambourne & Bryer	1961
	angle of incidence	Peckham/Elle	1958
	pitch rate (ramp test)	LeMay et al	1990
	pitch amplitude (ramp/oscillatory test)	Atta	1987
	reduced frequency (oscillatory test)	Gad-El-Hak & Ho	1985
	mean incidence (oscillatory test)	Huyer et al	1992
	sideslip/yaw	Grismer & Nelson	1995
	roll	Er-El et al	1989
	Strouhal number	Gad-El-Hak & Ho	1985
Vortex control	along-core blowing	Kuo & Lu	1995
	leading-edge suction/blowing	Gad-El-Hak & Ho	1985
	trailing-edge suction	Chiang & Zhong	1996

Table (A.1) - Summary Of Previous Experimental Work (Test Parameters)

APPENDIX B - Summary Of Previous Theoretical Work

Category	Theory	Who	Date
Instability	axisymmetric disturbances	Jones	1960
	"	Ludwieg	1965
	spiral disturbances	Lessen et al	1974
	non-linear interactions	Garg & Leibovich	1979
	"	Escudier	1982
Stagnation	separation analogy	Polhamus	1971
	"	Hall	1972
	failure of slender core/quasi-cylindrical approximation	Gartshore	1962
	"	Hall	1964
	"	Bossel	1969
	"	Mager	1972
	numerical failure	Kopecky & Torrance	1973
	"	Grabowski & Berger	1976
Wave phenomena	solitary waves	Benjamin	1962
	inertia waves	Leibovich	1970
	transition between conjugate-flow states	Squire	1960
	shock/hydraulic jump analogy	Benjamin	1962
Vorticity	negative azimuthal vorticity	Brown & Lopez	1990
	"	Boffadossi	1996

Table (B.1) - Summary Of Previous Theoretical Work

APPENDIX C - Layout Of Run Information Block

RIB Location	Static	Oscillatory	Ramp Up	Ramp Down
0	Run Number			
1	Date Of Test : Day			
2	Date Of Test : Month			
3	Date Of Test : Year			
4	Ambient Temperature (° C)			
5	Barometric Pressure (mm Hg)			
6	Motion Type (0)	Motion Type (1)	Motion Type (2)	Motion Type (3)
7	Starting Incidence (°)	Mean Incidence (°)	Starting Incidence (°)	
8	Arc (°)	Amplitude (°)	Ramp Arc (°)	
9	Empty	Oscillation Frequency (Hz)	Linear Pitch Rate (° /s)	
10	Number Of Samples In One Block			
11	Number Of Total Samples			
12	Number Of Data Blocks (Cycles)			
13	Sampling Frequency (Hz)			
14	Dynamic Pressure (PSI)			
15	Reynolds Number			
16	Mach Number			
17	Empty	Reduced Frequency	Reduced Pitch Rate	
18	Incoming Velocity (m/s)			
19	Dynamic Pressure (N/m^2)			
20	Model Number			
21	File ID			

Table (C.1) - Layout Of Run Information Block

APPENDIX D - Summary Of Wind-Tunnel Test Information

Motion Type : Static		Model Type : Sharp-nosed Delta Wing	
Run Number	Reynolds Number	Start Angle (°)	End Angle (°)
18000011	1.5×10^6	-5	10
18000021	1.5×10^6	11	26
18000031	1.5×10^6	27	42
18000041	1.0×10^6	-5	10
18000051	1.0×10^6	11	26
18000061	1.0×10^6	27	42

Table (D.1) - Summary Of Static Test Information

Motion Type : Oscillatory		Model Type : Sharp-nosed Delta Wing		
Run Number	Reynolds Number	Mean Angle (°)	Peak Amplitude (°)	Frequency (Hz)
18010891	1.5×10^6	5	10	0.379
18010901	1.5×10^6	5	10	1.895
18010911	1.5×10^6	5	10	3.789
18010921	1.5×10^6	5	10	4.926
18010931	1.5×10^6	5	10	5.911
18010941	1.5×10^6	5	10	6.897
18010951	1.5×10^6	10	10	0.379
18010961	1.5×10^6	10	10	1.895
18010971	1.5×10^6	10	10	3.789

Table (D.2) - Summary Of Oscillatory Test Information (page 1 of 3)

Motion Type : Oscillatory		Model Type : Sharp-nosed Delta Wing		
Run Number	Reynolds Number	Mean Angle (°)	Peak Amplitude (°)	Frequency (Hz)
18010981	1.5×10^6	10	10	4.926
18010991	1.5×10^6	10	10	5.911
18011001	1.5×10^6	10	10	6.897
18011011	1.5×10^6	15	10	0.379
18011021	1.5×10^6	15	10	1.895
18011031	1.5×10^6	15	10	3.789
18011041	1.5×10^6	15	10	4.926
18011051	1.5×10^6	15	10	5.911
18011061	1.5×10^6	15	10	6.897
18011071	1.5×10^6	20	10	0.379
18011081	1.5×10^6	20	10	1.895
18011091	1.5×10^6	20	10	3.789
18011101	1.5×10^6	20	10	4.926
18011111	1.5×10^6	20	10	5.911
18011121	1.5×10^6	20	10	6.897
18011131	1.5×10^6	25	10	0.379
18011141	1.5×10^6	25	10	1.895
18011151	1.5×10^6	25	10	3.789
18011161	1.5×10^6	25	10	4.926
18011171	1.5×10^6	25	10	5.911
18011181	1.5×10^6	25	10	6.897

Table (D.2) - Summary Of Oscillatory Test Information (page 2 of 3)

Motion Type : Oscillatory		Model Type : Sharp-nosed Delta Wing		
Run Number	Reynolds Number	Mean Angle (°)	Peak Amplitude (°)	Frequency (Hz)
18011192	1.5×10^6	5	10	3.789
18011202	1.5×10^6	10	10	3.789
18011212	1.5×10^6	15	10	3.789
18011222	1.5×10^6	20	10	3.789
18011232	1.5×10^6	25	10	3.789
18011241	1.5×10^6	20	20	0.379
18011251	1.5×10^6	20	20	1.895
18011261	1.5×10^6	20	20	3.789
18011271	1.5×10^6	30	10	0.379
18011281	1.5×10^6	35	10	0.379
18011291	1.5×10^6	30	10	1.895
18011301	1.5×10^6	35	10	1.895
18011311	1.5×10^6	30	10	3.789
18011321	1.5×10^6	35	10	3.789
18011331	1.5×10^6	30	10	4.926
18011341	1.5×10^6	35	10	4.926
18011351	1.5×10^6	30	10	5.911
18011361	1.5×10^6	35	10	5.911
18011371	1.5×10^6	30	10	6.897
18011381	1.5×10^6	35	10	6.897
End Of Test				

Table (D.2) - Summary Of Oscillatory Test Information (page 3 of 3)

Motion Type : Ramp Up		Model Type : Sharp-nosed Delta Wing		
Run Number	Reynolds Number	Start Angle (°)	End Angle (°)	Ramp Rate (° /s)
18020071	1.5×10^6	-5	40	1.36
18020081	1.5×10^6	-5	40	4.09
18020091	1.5×10^6	-5	40	6.82
18020101	1.5×10^6	-5	40	12.28
18020111	1.5×10^6	-5	40	23.19
18020121	1.5×10^6	-5	40	47.75
18020131	1.5×10^6	-5	40	70.94
18020141	1.5×10^6	-5	40	94.13
18020151	1.5×10^6	-5	40	118.60
18020161	1.5×10^6	-5	40	141.88
18020171	1.5×10^6	-5	40	158.25
18020181	1.5×10^6	-5	40	181.44
18020191	1.5×10^6	-5	40	195.80
18020201	1.5×10^6	-5	40	208.72
18020211	1.5×10^6	-5	40	234.64
18020221	1.5×10^6	-5	40	255.10
18020231	1.5×10^6	-5	40	276.93
18020241	1.5×10^6	-5	40	296.03
18020251	1.5×10^6	-5	40	313.76
18020261	1.5×10^6	-5	40	330.13
18020271	1.5×10^6	-5	40	345.14

Table (D.3) - Summary Of Ramp Up Test Information (page 1 of 3)

Motion Type : Ramp Up		Model Type : Sharp-nosed Delta Wing		
Run Number	Reynolds Number	Start Angle (°)	End Angle (°)	Ramp Rate (° /s)
18020281	1.5 x 10^6	-5	40	360.14
18020291	1.5 x 10^6	-5	40	373.79
18020301	1.5 x 10^6	-5	40	392.89
18020311	1.5 x 10^6	-5	40	411.98
18020321	1.5 x 10^6	-5	40	425.64
18020331	1.5 x 10^6	-5	40	439.27
18020341	1.5 x 10^6	-5	40	458.37
18020351	1.5 x 10^6	-5	40	476.10
18020361	1.5 x 10^6	-5	40	482.92
18020372	1.5 x 10^6	-5	40	118.60
18020382	1.5 x 10^6	-5	40	141.88
18020392	1.5 x 10^6	-5	40	158.25
18020402	1.5 x 10^6	-5	40	181.44
18020412	1.5 x 10^6	-5	40	195.80
18020422	1.5 x 10^6	-5	40	208.72
18020432	1.5 x 10^6	-5	40	234.64
18020442	1.5 x 10^6	-5	40	255.10
18020452	1.5 x 10^6	-5	40	276.93
18020462	1.5 x 10^6	-5	40	296.03
18020472	1.5 x 10^6	-5	40	313.76
18020482	1.5 x 10^6	-5	40	330.13

Table (D.3) - Summary Of Ramp Up Test Information (page 2 of 3)

Motion Type : Ramp Up		Model Type : Sharp-nosed Delta Wing		
Run Number	Reynolds Number	Start Angle (°)	End Angle (°)	Ramp Rate (° /s)
18020492	1.5×10^6	-5	40	345.14
18020502	1.5×10^6	-5	40	360.14
18020512	1.5×10^6	-5	40	373.79
18020522	1.5×10^6	-5	40	392.89
18020532	1.5×10^6	-5	40	411.98
18020542	1.5×10^6	-5	40	425.64
18020552	1.5×10^6	-5	40	439.27
18020562	1.5×10^6	-5	40	458.37
18020572	1.5×10^6	-5	40	476.10
18020582	1.5×10^6	-5	40	482.92
End Of Test				

Table (D.3) - Summary Of Ramp Up Test Information (page 3 of 3)

Motion Type : Ramp Down		Model Type : Sharp-nosed Delta Wing		
Run Number	Reynolds Number	Start Angle (°)	End Angle (°)	Ramp Rate (° /s)
18030591	1.0×10^6	40	-5	1.36
18030601	1.0×10^6	40	-5	4.09
18030611	1.0×10^6	40	-5	6.82
18030621	1.0×10^6	40	-5	12.28
18030631	1.0×10^6	40	-5	23.19
18030641	1.0×10^6	40	-5	47.75
18030651	1.0×10^6	40	-5	70.94

Table (D.4) - Summary Of Ramp Down Test Information (page 1 of 2)

Motion Type : Ramp Down		Model Type : Sharp-nosed Delta Wing		
Run Number	Reynolds Number	Start Angle (°)	End Angle (°)	Ramp Rate (° /s)
18030661	1.0×10^6	40	-5	94.13
18030671	1.0×10^6	40	-5	118.60
18030681	1.0×10^6	40	-5	141.88
18030691	1.0×10^6	40	-5	158.25
18030701	1.0×10^6	40	-5	181.44
18030711	1.0×10^6	40	-5	195.80
18030721	1.0×10^6	40	-5	208.72
18030731	1.0×10^6	40	-5	234.64
18030741	1.0×10^6	40	-5	255.10
18030751	1.0×10^6	40	-5	276.93
18030761	1.0×10^6	40	-5	296.03
18030771	1.0×10^6	40	-5	313.76
18030781	1.0×10^6	40	-5	330.13
18030791	1.0×10^6	40	-5	345.14
18030801	1.0×10^6	40	-5	360.14
18030811	1.0×10^6	40	-5	373.79
18030821	1.0×10^6	40	-5	392.89
18030831	1.0×10^6	40	-5	411.98
18030841	1.0×10^6	40	-5	425.64
18030851	1.0×10^6	40	-5	439.27
18030861	1.0×10^6	40	-5	458.37
18030871	1.0×10^6	40	-5	476.10
18030881	1.0×10^6	40	-5	482.92
End Of Test				

Table (D.4) - Summary Of Ramp Down Test Information (page 2 of 2)

BIBLIOGRAPHY

Ashley, H., J. Katz, et al. (1991). "Survey of research on unsteady aerodynamic loading of delta wings." Journal of Fluids & Structures: 363-390.

Atta, R. and D. Rockwell (1990). "Leading-edge vortices due to low Reynolds number flow past a pitching delta wing." AIAA Journal **28**(6): 995-1004.

Benjamin, T. B. (1962). "Theory of the vortex breakdown phenomenon." Journal of Fluid Mechanics **14**: 593-629.

Berndt, S. B. (1950). "Wind-tunnel interference due to lift for delta wings of small aspect ratio." Technical Note, Royal Institute of Technology, Stockholm, Sweden.

Boffadossi, M. (1996). "Calculation of vortex breakdown over a delta wing by a vortex-lattice method." 20th Congress of the International Council of the Aeronautical Sciences, Sorrento, Napoli, Italy, ICAS.

Bossel, H. H. (1969). "Vortex breakdown flowfield." Physics of Fluids **12**(3): 498-508.

Brown, G. L. and J. M. Lopez (1990). "Axisymmetric vortex breakdown, Part 2 - Physical mechanisms." Journal of Fluid Mechanics **221**: 553-576.

Chiang, S. and D. Zhong (1996). "Trailing-edge jet control of leading-edge vortices of a delta wing." AIAA Journal **34**(7): 1447-1457.

Cipolla, K. M. and D. Rockwell (1995). "Flow structure on a stalled delta wing subjected to small amplitude pitching oscillations." AIAA Journal **33**(7): 1256-1262.

Delery, J. M. (1994). "Aspects of vortex breakdown." Progress in Aerospace Sciences **30**: 1-59.

Elle, B. J. (1958). "An investigation at low speed of the flow near the apex of thin delta wings with sharp leading edges." Reports and Memoranda, No. 3176, Aeronautical Research Council, .

Elle, B. J. (1960). "On the breakdown at high incidences of the leading-edge vortices on delta wings." Journal of the Royal Aeronautical Society **64**(April): 491-493.

Er-El, J., D. Seter, et al. (1989). "Non-linear aerodynamics of a delta wing in combined pitch and roll." Journal Of Aircraft **26**(3): 254-259.

Escudier, M. (1988). "Vortex breakdown : Observations and explanations." Progress in Aerospace Sciences **25**: 189-229.

Faler, J. H. and S. Leibovich (1977). "Disrupted states of vortex flow and vortex breakdown." Physics of Fluids **20**(9): 1385-1400.

continued...

Gad-el-Hak, M. and C.-M. Ho (1985). "The pitching delta wing." AIAA Journal **23**(11): 1660-1665.

Garg, A. K., S. Leibovich (1979). "Spectral characteristics of vortex breakdown flowfields." Physics of Fluids **22**: 2053-2064.

Gartshore, I. S. (1962) "Recent work in swirling incompressible flow." National Research Council of Canada Report No. 6968 (formerly National Aeronautical Establishment Report No. LR-343).

Grabowski, W. J. B., S. A. Berger (1976). "Solutions of the Navier-Stokes equations for vortex breakdown." Journal of Fluid Mechanics **75**(3): 525-544.

Greenwell, D. I. and N. J. Wood (1992). "Determination of vortex burst location on delta wings from surface pressure measurements." AIAA Journal **30**(11): 2736-2739.

Greenwell, D. I. and N. J. Wood (1994). "Some observations on the dynamic response to wing motion of the vortex burst phenomenon." Aeronautical Journal **98**(2): 49-59.

Grismer, D. S. and R. C. Nelson (1995). "Double-delta wing aerodynamics for pitching motions with & without sideslip." Journal of Aircraft **32**(6): 1303-1311.

Guglieri, G. and F. B. Quagliotti (1997). "Experimental investigation of vortex dynamics on a 65 degree delta wing in sideslip." The Aeronautical Journal **101**(Mar): 111-120.

Gursul, I. and C.-M. Ho (1993). "Vortex breakdown over delta wings in unsteady freestream." AIAA Journal **32**(2): 433-436.

Gursul, I. and H. Yang (1995). "Vortex breakdown over a pitching delta wing." Journal of fluids & structures **1995**(9): 571-583.

Hall, M. G. (1964). "The structure of concentrated vortex cores." Progress in Aeronautical sciences **7**: 53-110.

Hall, M. G. (1972). "Vortex breakdown." Annual Review of Fluid Mechanics **4**: 195-218.

Harvey, J. K. (1960). "Some observations of the vortex breakdown phenomenon." Journal of fluid mechanics **14**: 585-592.

Hemsch, M. J. and J. M. Luckring (1990). "Connection between leading-edge sweep, vortex lift and vortex strength for delta wings. (Eng. Note)." Journal of Aircraft **27**(5): 473-475.

Hummel, D. and P. S. Srinivasan (1967). "Vortex breakdown effects on the low speed aerodynamic characteristics of slender delta wings in symmetrical flow." Journal of the Royal Aeronautical Society **71**(April): 319-322.

continued...

Huyer, S. A., M. C. Robinson, et al. (1992). "Unsteady aerodynamic loading produced by a sinusoidally oscillating delta wing." Journal of Aircraft **29**(3): 366-373.

Jarrah, M. A. M. (1989). "Low-speed wind-tunnel investigation of flow about delta wings, oscillating in pitch to very high angle of attack." AIAA Report No. 89-0295.

Jones, J. P. (1960). "The breakdown of vortices in separated flow." U.S.A.A. Report No. 140.

Kegelman, J. T., F. W. Roos (1989). "Effect of leading-edge shape and vortex burst on the flowfield of a 70 degree sweep delta wing." AIAA Report No. 89-0086.

Kopecky, R. M., K. E. Torrance (1973). "Initiation and structure of axisymmetric eddies in a rotating stream." Computers & Fluids **1**: 289-300.

Kuo, C. H. and N.-Y. Lu (1995). "Vortex characteristics over delta wings subject to transient along-core blowing." AIAA Journal **33**(12): 2418-2420.

Lambourne, N. C. and D. W. Bryer (1961). "The bursting of leading-edge vortices - some observations & discussion of the phenomenon." Reports & Memoranda, No. 3282, Aeronautical Research Council.

Lee, M. and C.-M. Ho (1990). "Lift force of delta wings." Applied Mechanics Review **43**(9): 209-221.

Leibovich, S. (1978). "The structure of vortex breakdown." Annual Review of Fluid Mechanics **10**: 221-246.

LeMay, S. P., S. M. Batill, et al. (1990). "Vortex dynamics on a pitching delta wing." Journal of Aircraft **27**(2): 131-138.

Lessen, M., P. J. Singh, et al. (1974). "The stability of a trailing line vortex, part 1 : Inviscid theory." Journal of Fluid Mechanics **63**(4): 753-763.

Lowson, M. V. (1963). "The separated flows on slender wings in unsteady motion." Reports & Memoranda, No. 3448, Aeronautical Research Council.

Lowson, M. V. (1964). "Some experiments with vortex breakdown." Journal of the Royal Aeronautical Society **68**(May): 343-346.

Lowson, M. V. (1991). "Visualisation measurements of vortex flows." Journal of Aircraft **28**(5): 320-327.

Lowson, M. V. and A. J. Riley (1995). "Vortex breakdown control by delta wing geometry." Journal of Aircraft **32**(4): 832-838.

continued...

Ludwieg, H. (1965). "Erklarung des wirbellaufplatzens mit hilfe der stabilitatstheorie fur stromungenmit schraubenlinienformigen stromlinien." Zeitschrift fur Flugwissenschaften **13**. 437-442.

Mabey, D. G. (1991). "Review of aircraft dynamic loads due to flow separation." AGARD CP494, AGARD.

Mager, A. (1972). "Dissipation & breakdown of a wing-tip vortex." Journal of Fluid Mechanics **55**(4): 609-628.

Magness, C. L. (1991). "Unsteady response of the leading-edge vortices on a pitching delta wing." PhD Dissertation, Lehigh University, Bethlehem, PA.

McKernan, J. F., F. M. Payne, et al. (1988). "Vortex breakdown measurements on a 70 deg sweepback delta wing." Journal of Aircraft **25**(11): 991-992.

Nelson, R. C. (1991). "Unsteady aerodynamics of slender wings." AGARD Report No. 776, AGARD.

Nelson, R. C. and K. D. Visser (1991). "Breaking down the delta wing vortex - the role of vorticity in the breakdown process." AGARD CP494.

Panton, R. L. (1990). "Effects of a contoured apex on vortex breakdown." AIAA Journal **27**(3): 285-288.

Parker, A. G. (1976). "Aerodynamic characteristics of slender wings with sharp leading edges - A review." Journal of Aircraft **13**(3): 161-168.

Payne, F. M., T. T. Ng, et al. (1987). "Experimental study of the velocity field on a delta wing." AIAA Report No. 87-1231, AIAA.

Payne, F. M., T. T. Ng, et al. (1986). "Visualisation & flow surveys of the leading-edge vortex structure on delta wing planforms." AIAA Report No. 86-0330, AIAA.

Peckham, D. H. (1958). "Low speed wind tunnel tests on a series of uncambered slender pointed wings with sharp edges." Reports and Memoranda No. 3186, Aeronautical Research Council.

Peckham, D. H. and S. A. Atkinson (1957). "Preliminary results of low speed wind tunnel tests on a gothic wing of AR = 1.0." Current Papers, CP508, Aeronautical Research Council.

Polhamus, E. C. (1971). "Predictions of vortex-lift characteristics by a leading-edge suction analogy." Journal of Aircraft **8**(4): 193-199.

Spall, R. E., T. B. Gatski, et al. (1987). "A criterion for vortex breakdown." Physics of Fluids **30**(11): 3434-3440.

continued...

Squire, H. B. (1960). "Analysis of the vortex breakdown phenomenon." Report No. 102, Imperial College of Science & Technology, London. .

Thompson, S. A., S. M. Batill, et al. (1990). "Delta wing surface pressures for high angle of attack manoeuvres." AIAA Report No. 90-2813.

Weinberg, Z. (1992). "Effect of tunnel walls on vortex breakdown location over delta wings." AIAA Journal **30**(6): 1584-1586.

Wentz, W. H. and D. L. Kohlman (1971). "Vortex breakdown on slender sharp-edged wings." AIAA Report No. 69-778.

Yegna Narayan, K. and S. N. Seshadri (1997). "Types of flow on the leeside of delta wings." Progress in Aerospace Sciences **33**(3/4): 167-257.

Zohar, Y. and J. Er-El (1988). "Influence of the aspect ratio on the aerodynamics of the delta wing at high angle of attack." Journal of Aircraft **25**(3): 200-205.